Plant Biotechnology Journal
Open Access

Plant Biotechnology Journal (2024), pp. 1–16 doi: 10.1111/pbi.14474

A gain-of-function mutation at the C-terminus of FT-D1 promotes heading by interacting with 14-3-3A and FDL6 in wheat

Yuting Li[1,2], Hongchun Xiong[1,*], Huijun Guo[1], Yongdun Xie[1], Linshu Zhao[1], Jiayu Gu[1], Huiyuan Li[1], Shirong Zhao[1], Yuping Ding[1], Chunyun Zhou[1], Zhengwu Fang[2] and Luxiang Liu[1,*]

[1]*State Key Laboratory of Crop Gene Resources and Breeding/National Engineering Laboratory of Crop Molecular Breeding/CAEA Research and Development Centre on Nuclear Technology Applications for Irradiation Mutation Breeding, Institute of Crop Sciences, Chinese Academy of Agricultural Sciences, Beijing, 100081, China*
[2]*MARA Key Laboratory of Sustainable Crop Production in the Middle Reaches of the Yangtze River (co-construction by Ministry and Province), College of Agriculture, Yangtze University, Jingzhou, 434025, China*

Received 28 April 2024;
revised 17 July 2024;
accepted 31 August 2024.
**Correspondence* (Tel +86-1062122719; fax +86-1082108543; email liuluxiang@caas.cn (L.L.) and Tel +86-1082108575; fax +86-1082108543; email xionghongchun@caas.cn (H.X.))

Keywords: wheat, FT-D1, heading date, plant height, FAC, ELF5.

Summary

Vernalization and photoperiod pathways converging at *FT1* control the transition to flowering in wheat. Here, we identified a gain-of-function mutation in *FT-D1* that results in earlier heading date (HD), and shorter plant height and spike length in the gamma ray-induced *eh1* wheat mutant. Knockout of the wild-type and overexpression of the mutated *FT-D1* indicate that both alleles are functional to affect HD and plant height. Protein interaction assays demonstrated that the frameshift mutation in FT-D1^{eh1} exon 3 led to gain-of-function interactions with 14-3-3A and FDL6, thereby enabling the formation of florigen activation complex (FAC) and consequently activating a flowering-related transcriptomic programme. This mutation did not affect *FT-D1*^{eh1} interactions with TaNaKR5 or TaFTIP7, both of which could modulate HD, potentially via mediating FT-D1 translocation to the shoot apical meristem. Furthermore, the 'Segment B' external loop is essential for FT-D1 interaction with FDL6, while residue Y85 is required for interactions with TaNaKR5 and TaFTIP7. Finally, the flowering regulatory hub gene, *ELF5*, was identified as the *FT-D1* regulatory target. This study illustrates *FT-D1* function in determining wheat HD with a suite of interaction partners and provides genetic resources for tuning HD in elite wheat lines.

Introduction

Common wheat (*Triticum aestivum* L.) is among the most widely cultivated cereal crops, providing ~20% of the calories and protein consumed by humans worldwide (Dubcovsky and Dvorak, 2007; Pfeifer *et al*., 2014). Heading date (HD; flowering time) is a complex quantitative trait that determines the transition from vegetative phase to reproductive growth in cereal crops (Kiseleva and Salina, 2018). In wheat, several regulatory pathways synchronize HD with environmental cues to ensure optimal flowering time, a key factor in wheat adaptability (Distelfeld *et al*., 2009a; Kamran *et al*., 2014). Identifying HD-related genes and characterizing their function is essential to understanding the regulation of wheat adaptation and subsequently improving yield and regionally suitable varieties.

In wheat, both endogenous genetic elements and external environmental signals control HD. Long-day (LD) conditions induce wheat flowering, whereas variations in *photoperiod* genes, such as *Ppd1*, enable switching to reproductive growth under short days (Beales *et al*., 2007; Shaw *et al*., 2012; Wilhelm *et al*., 2009). Depending on its requirements for prolonged cold exposure, wheat can be classified into winter or spring growth habits through the activity of *vernalization* (*VRN*) genes (Dubcovsky *et al*., 1998; Goncharov, 2004; Wu *et al*., 2022a). The first cloned *VRN1* gene, encoding an *APETALA1-like* MADS-box transcription factor, functions as the main factor initiating flowering (Yan *et al*., 2003). Alternatively, *VRN2* locus includes two linked zinc-finger and CCT domain-containing genes that maintain high expression levels in non-vernalized winter wheat to repress flowering (Distelfeld *et al*., 2009b; Yan *et al*., 2004). In wheat and barley, *VRN3* is an orthologue of *Arabidopsis Flowering locus T* (*FT*), also known as *TaFT1* (Yan *et al*., 2006). In wheat HD regulatory networks, *FT1* plays a central role in integrating vernalization cues with photoperiod and other environmental signals (Distelfeld *et al*., 2009a). The previous studies have identified frameshift-inducing variations in exon 3 of *FT-D1* associated with HD, which could potentially introduce a novel attachment site for lipoprotein (Bonnin *et al*., 2007; Li *et al*., 2017). However, the molecular mechanism through which these variations in the *FT-D1* coding region could affect its function remains unclear.

In *Arabidopsis*, *FT* encodes a phosphatidylethanolamine-binding protein that serves as a component of the florigen (Corbesier *et al*., 2007; Mathieu *et al*., 2007). FT is translocated from leaves to the shoot apical meristem (SAM), where it interacts with the bZIP transcription factor, FD, to promote floral transition by activating floral meristem identity genes (Abe *et al*., 2005; Wigge *et al*., 2005). In rice, crystal structure analyses suggest that the FT orthologue,

Please cite this article as: Li, Y., Xiong, H., Guo, H., Xie, Y., Zhao, L., Gu, J., Li, H., Zhao, S., Ding, Y., Zhou, C., Fang, Z. and Liu, L. (2024) A gain-of-function mutation at the C-terminus of FT-D1 promotes heading by interacting with 14-3-3A and FDL6 in wheat. *Plant Biotechnol. J.*, https://doi.org/10.1111/pbi.14474.

Hd3a, interacts with a 14-3-3 protein, GF14c, to recruit OsFD1, and together form a heterohexameric FAC (Taoka *et al.*, 2011). Investigation of FT structure has identified several key elements affecting its floral induction activity. For example, the 'Segment B' external loop was found to be important to FT activity, potentially via recognition of interaction partners (Ahn *et al.*, 2006). Additionally, the Y85H conversion in FT can abolish its positive regulation of flowering (Hanzawa *et al.*, 2005). As a small transcription co-factor, FT requires other molecular chaperones for long-distance translocation to the SAM (Giakountis and Coupland, 2008). FTIP1, a multiple C2 domain and transmembrane region protein family member, is essential for FT movement from companion cells to sieve elements in *Arabidopsis* (Liu *et al.*, 2012). In sieve elements, a heavy-metal-associated domain-containing protein, NaKR1, transports FT to the SAM via phloem (Zhu *et al.*, 2016).

To define the molecular functions and protein properties of wheat FT1, in this current study, we identified a gain-of-function mutation in *FT-D1* that conferred multifaceted effects on HD, plant height, and spike length in the *eh1* early heading wheat mutant. We further demonstrated that the mutant allele of *FT-D1* in *eh1* acquired competence to interact with 14-3-3A and FDL6 that is absent in the wild-type allele, consequently regulating the expression of downstream floral genes. Our results suggest that wild-type *FT-D1* regulates HD to a lesser extent, suggesting reduced function compared to the mutant, and could interact with the TaNaKR5 and TaFTIP7 transport proteins, disrupting either of which alters HD, potentially by reducing FT-D1 transport. Furthermore, we identified key elements in FT-D1 essential for its interactions with different proteins, and finally, we defined genes that were differentially regulated by different *FT-D1* alleles, such as *ELF5* and *FY*. These results not only provide a comprehensive perspective of the mechanistic molecular basis of *FT-D1* function, but also generate valuable genetic resources for wheat breeding programmes focused on adaptation and flowering time in elite varieties.

Results

A frameshift mutation in *FT-D1* contributes to early heading in the *eh1* wheat mutant

We previously identified a gamma-ray-induced wheat mutant, *eh1*, that exhibits an early heading phenotype (Li *et al.*, 2020), and matures 4–5 days earlier than wild-type (WT, ZY9, Figure S1a). Genetic analysis suggested a partial-dominant effect of the early heading phenotype in the *eh1* mutant (Degree of dominance = 0.20, Figure S1b). Additionally, the *eh1* mutant displays significant reductions of plant height and spike length by 26.9% and 26.1% ($P < 0.01$), respectively, while spikelet number per spike in *eh1* is not significantly affected compared to the WT plants (Figure S1c–f). To determine the genetic basis of the *eh1* phenotype, we performed bulked segregant analysis (BSA) with extremely early and late heading plants in the F_2 population generated by crossing *eh1* with WT. This analysis revealed two loci significantly associated with HD on chromosomes 2D and 7D, respectively (Figure 1a,b). Based on its strong association with HD, the putative locus on chromosome 7D was selected for further analysis. We subsequently constructed a linkage map with 12 KASP markers that spanned 79.2 cM on chromosome 7D. By incorporating HD phenotype data, a significant QTL with a LOD > 35 was identified between KASP markers *S10* and *E32* that could explain 16.4% of the HD variation in the F_2 population (Figure 1c). The flanking markers spanned a 1.65 Mb interval that contained 16 high-confidence annotated genes in the Chinese Spring reference genome (IWGSC, 2018). Annotation of variants identified only one gene, *FT-D1* (*TraesCS7D02G111600*), which harboured a single nucleotide insertion in exon 3 that could induce a frameshift in downstream protein coding sequence (Table S1). After validating this *FT-D1* variant by Sanger sequencing (Figure 1d), the phenotypic analysis indicated that homozygous *FT-D1*^{eh1} plants had an average HD approximately 3 days earlier than *FT-D1*^{WT} plants (Figure 1e). To further investigate the effects of *FT-D1*^{eh1} on HD, we performed reciprocal backcrosses of *FT-D1*^{eh1} with WT plants and constructed two BC_2F_2 lines. Phenotyping of these BC_2F_2 lines revealed that the HD of plants harbouring the *FT-D1*^{eh1} allele was 3–5 days earlier than that of WT. Additionally, plant height and spike length were reduced by 13.6% and 22.4% in the BC_2F_2 lines, respectively (Figure S2a,b). Consistent with these results, phenotypic analysis of the F_2-derived F_3 lines showed that HD, plant height, spike length, and spikelet number per spike in *FT-D1*^{eh1} plants were, respectively, reduced by 4 days, 8.3%, 13.5%, and 6.1% compared to *FT-D1*^{WT} lines (Figure S2c). These results suggested that the frameshift mutation in *FT-D1*^{eh1} not only promoted earlier HD in the *eh1* mutant, but also affected plant height and spike length. We then examined *FT-D1* expression patterns in different growth stages and found that its transcript levels were relatively low during vegetative growth, but gradually increased upon transition to reproductive development. Notably, *FT-D1* expression levels were similar between *eh1* and WT plants at different developmental stages (Figure 1f). Additionally, the *FT-D1* expression was preferentially induced by long-day (LDs) conditions, and both *FT-D1* alleles from *eh1* and WT displayed similar, rhythmic expression patterns in response to LDs, except a relatively higher transcription of *FT-D1*^{eh1} than *FT-D*^{WT} when plants were switched to light conditions for 12–16 h (Figure 1g). Overall, these collective results showed that a frameshift mutation in exon 3 of *FT-D1* contributes to earlier heading, shorter plants, and reduced spike size in the *eh1* mutant wheat line.

Gain-of-function mutation in FT-D1^{eh1} leads to interaction with 14-3-3A and FDL6 to regulate flowering-related genes

We hypothesized that the phenotype associated with the *FT-D1*^{eh1} allele was likely due to functional changes caused by frameshift in the encoded protein. More specifically, the frameshift induced by the insertion in exon 3 altered 33.5% of the peptide sequence in *FT-D1*^{eh1}. Based on the reported interactions of FT with NaKR1 and FTIP1 required for its transport to the SAM and subsequent induction of flowering through interaction with the bZIP transcription factor, FD in *Arabidopsis* (Abe *et al.*, 2005; Liu *et al.*, 2012; Zhu *et al.*, 2016), we therefore searched the wheat reference genome (IWGSC, 2018) for *NaKR1* and *FTIP1* orthologues by homology search. This analysis identified *TaNaKR3*, *TaNaKR5*, *TaFTIP5*, and *TaFTIP7* based on their high identity in amino acid sequences. In addition, we selected two *FD*-like proteins, FDL2 and FDL6, and both were shown to interact with FT1 in wheat (Li and Dubcovsky, 2008). In Y2H assays, only FT-D1^{eh1} showed interaction with FDL6, as well as weak interactions with TaFTIP7, while both the *eh1* and WT alleles could interact with TaNaKR5 (Figure 2a). By contrast, GST pull-down assays indicated that neither FT-D1^{eh1} nor FT-D1^{WT} could interact with FDL6 *in vitro* (Figure 2b). As previous studies suggested that Hd3a (FT homologue in rice) interaction with

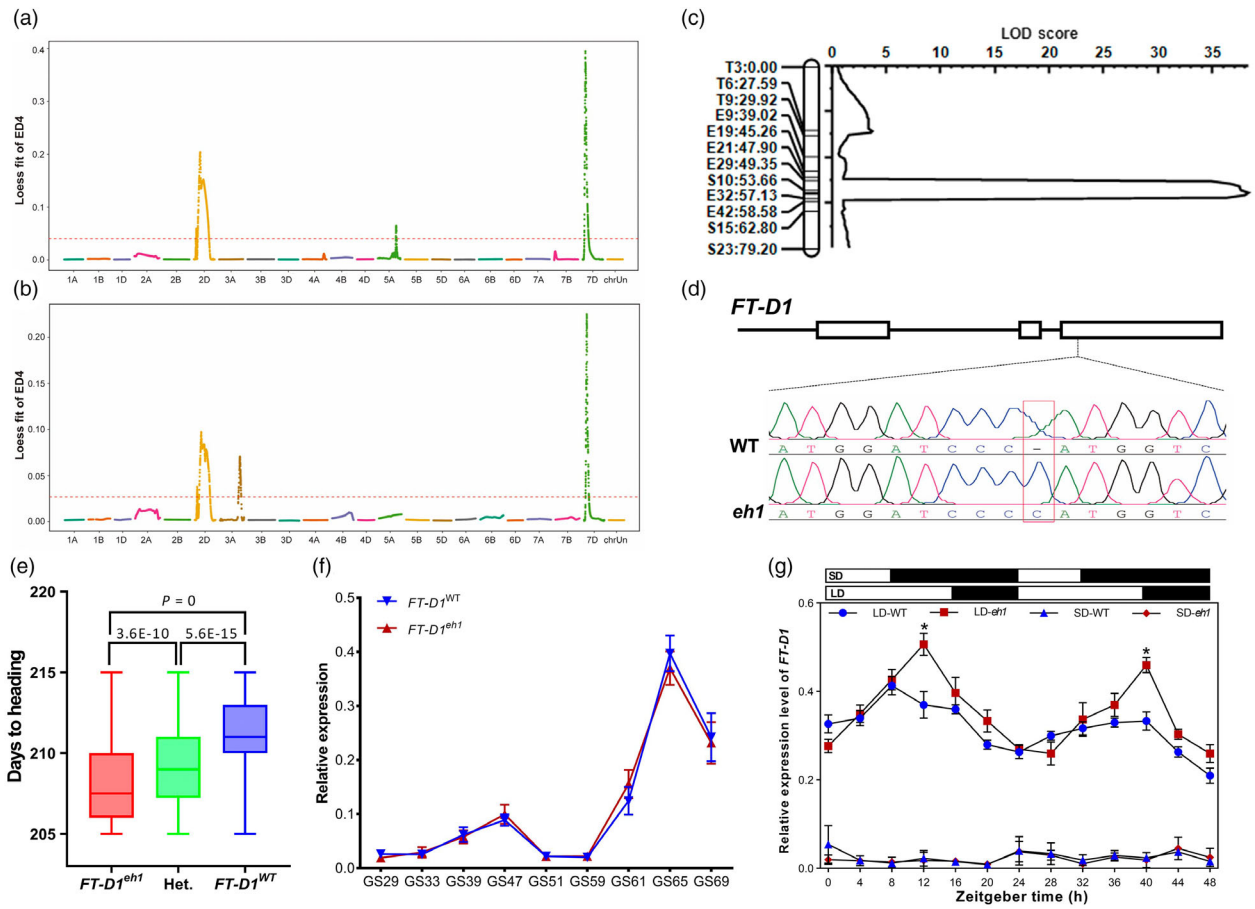

Figure 1 A single nucleotide insertion in *FT-D1* promoted HD in the *eh1* wheat mutant. (a, b) Association analysis based on DNA bulks from extremely early and late heading F_2 plants. Two biological replicates were performed to filter out false positives. The dotted-red lines represent the 99th percentile of the fitted ED^4 value. (c) Validation of HD locus in the F_2 population by QTL mapping on chromosome 7D with 12 SNP-derived KASP markers. (d) Verification of the single nucleotide insertion in *FT-D1*^{eh1} by Sanger sequencing. The exons and introns were shown as rectangles and solid lines, respectively. The red rectangle in the Sanger diagram indicates, compared to the wild-type, a single base insertion at the third exon in *FT-D1*^{eh1}. (e) Comparison of average HD in F_2 plants with different *FT-D1* genotypes. (f) Expression profiling of *FT-D1* in *eh1* mutant and wild-type at different developmental stages. Leaf samples were collected at nine different growth stages according to the Zadoks scale system. Expression levels were normalized based on the endogenous control gene *Actin*. Error bars indicated the standard deviation of three biological replicates. (g) Rhythmic expression of *FT-D1*^{eh1} and *FT-D1*^{WT} under long-day (16 h light/8 h dark) and short-day (8 h light/16 h dark) conditions. Asterisks indicate significant differences based on the Student's *t*-test. *$P < 0.05$.

OsFD1 required a structural link mediated by the 14-3-3 protein, GF14c, *in vivo*, and that endogenous 14-3-3 proteins could mediate FT1-FDL2 interactions in yeast (Li *et al.*, 2015; Taoka *et al.*, 2011). We therefore examined possible interactions with 14-3-3A from wheat. In yeast cells, FT-D1^{eh1}, but not FT-D1^{WT}, could interact with wheat 14-3-3A, which also interacted with FDL6 (Figure 2d). This FT-D1^{eh1}–14-3-3A interaction was confirmed by GST pull-down assays (Figure 2c). Furthermore, BiFC assays showed that FT-D1^{eh1} could interact with FDL6 in the nucleus, and with 14-3-3A in the nucleus and cytoplasm, while 14-3-3A interacted with FDL6 only in the nucleus of tobacco leaves, and FT-D1^{WT} could not interact with either protein (Figure 2e). These protein interactions of FT-D1^{eh1}–14-3-3A, FT-D1^{eh1}-FDL6, and 14-3-3A-FDL6 were further validated by luciferase complementation imaging (LCI) assays (Figure 2f). These results collectively suggested that the frameshift mutation in FT-D1^{eh1} enabled its direct or indirect interaction with 14-3-3A and FDL6 to form the florigen activation complex (FAC). Additionally, GST pull-down, BiFC, and LCI assays also indicated that both the *eh1* and WT FT-D1 alleles could directly interact with TaNaKR5 and TaFTIP7 (Figure S3), suggesting that this mutation in FT-D1^{eh1} did not affect its physical interactions with these proteins. We then analysed the transcript levels of several flowering genes and found that *VRN1*, *FUL3*, *AGLG1*, *AGL29*, *SOC1*, and *Ppd1*, in particular, were significantly upregulated in young spikes of *eh1* plants compared with WT (Figure 2g). These results suggested that the frameshift in FT-D1^{eh1} led to gain-of-function that enabled interaction with 14-3-3A and FDL6 to form the FAC, consequently facilitating transcriptional regulation of downstream flowering-related genes.

Key residues in FT-D1 required for its protein interaction with different partners

As our above analyses highlighted the significance of FT-D1^{eh1} C-terminus interactions with 14-3-3A and FDL6, but not TaNaKR5 or TaFTIP7, we next sought to identify the FT-D1 protein regions responsible for its interactions with different proteins. Previous studies have indicated that a Tyr residue at position 85 (Y85) and a peptide region previously designated as 'Segment B' in the C-terminus both were important to FT function in floral induction

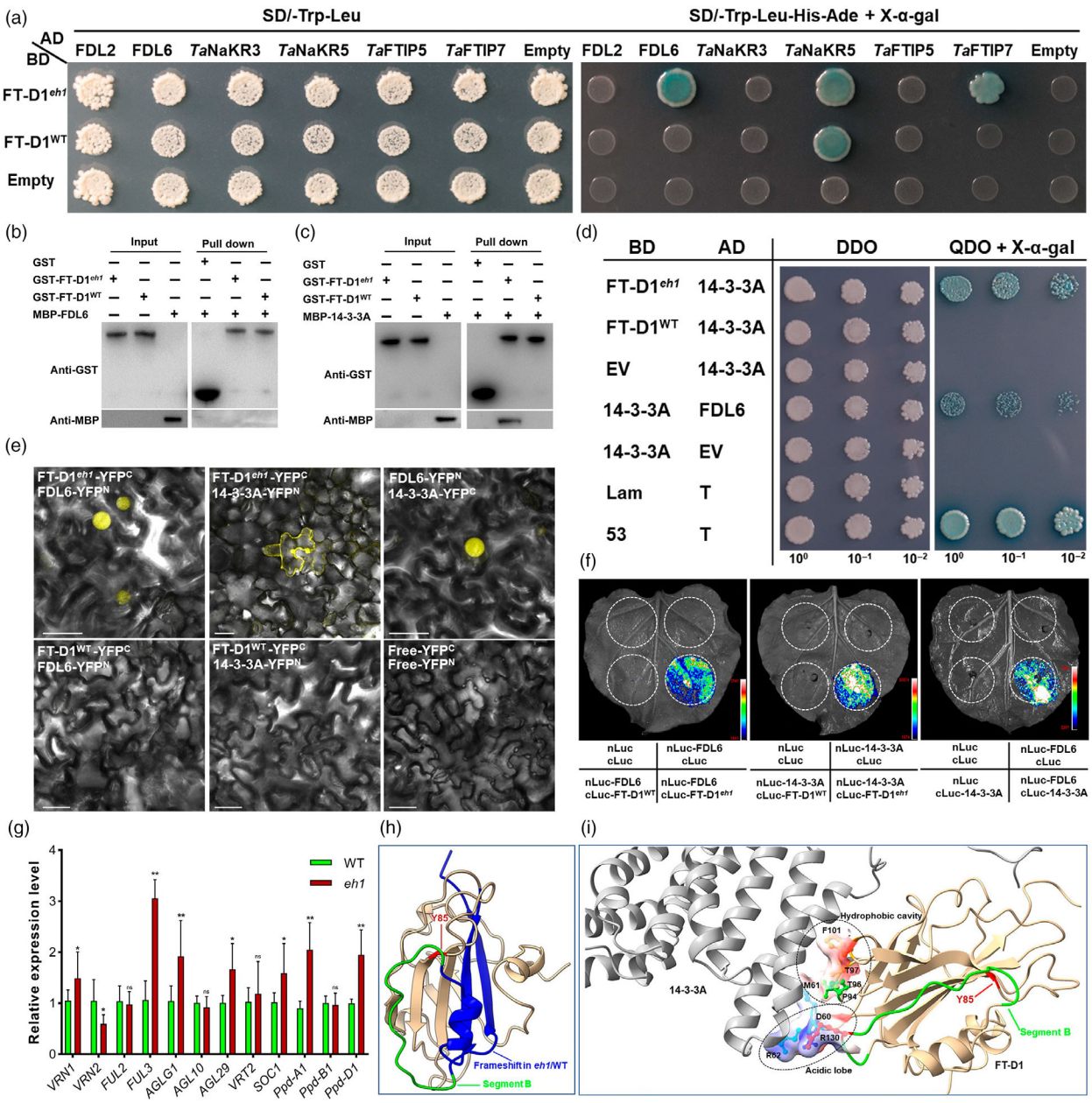

Figure 2 FT-D1^{eh1} interacted with 14-3-3A and FDL6 proteins to regulate the expression of flowering-related genes. (a) Yeast two-hybrid (Y2H) analysis of the interaction of FT-D1$^{eh1/WT}$ with FDL2, FDL6, TaNaKR3, TaNaKR5, TaFTIP5, and TaFTIP7. Yeast cells co-transformed with the BD-bait and AD-prey vectors were plated on SD/−Trp-Leu and SD/−Trp-Leu-His-Ade-X-α-gal. BD, pGBKT7; AD, pGADKT7. GST pull-down assays to analyse the interaction of FT-D1$^{eh1/WT}$ with MBP-FDL6 (b) and MBP-14-3-3A (c). GST- and MBP-tagged proteins were recognized by anti-GST and anti-MBP antibodies in the Western blot experiment, respectively. (d) Y2H assay analysis of FT-D1^{eh1} interacting with 14-3-3A protein, and 14-3-3A interacting with FDL6. The pGADT7-T was co-transformed with pGBKT7–53 or pGBKT7–Lam to serve as positive or negative controls, respectively. DDO, SD/−Trp-Leu; QDO, SD/−Trp-Leu-His-Ade. (e) Protein interaction analyses between FT-D1$^{eh1/WT}$ and 14-3-3A, FDL6; and between 14-3-3A and FDL6 as revealed by BiFC assays in tobacco leaves. Scale bar = 30 μm. (f) Luciferase complementation imaging (LCI) assays validated the protein interactions of FT-D1$^{eh1/WT}$-14-3-3A, FT-D1$^{eh1/WT}$-FDL6, and 14-3-3A-FDL6 in tobacco leaves. (g) Relative expression of 12 flowering-related genes in the spikes of *eh1* and WT plants at the heading stage. Data were shown as mean ± SD; *P* values were determined by two-tailed Student's *t*-test. *$P < 0.05$; **$P < 0.01$; ns, no significant difference. (h) Modelling of FT-D1 structure based on the rice Hd3a structure. The residue Y85, Segment B, and the frameshift mutation in *FT-D1*^{eh1} were highlighted with different colours. (i) Modelling FT-D1-14-3-3A interacting surfaces based on the rice FAC.

(Ahn *et al.*, 2006; Hanzawa *et al.*, 2005). These two-sequence elements are highly conserved among wheat FT-D1, *Arabidopsis* FT, and rice Hd3a (Figure S4). Therefore, we generated seven FT-D1 truncation variants to systematically exclude Y85, Segment B, and/or the exon 3 single nucleotide insertion in *FT-D1*^{eh1} individually or in combination (Figure S5a). The results of Y2H suggested that FT-D1^{eh1}-FDL6 interaction did not involve Y85, but required the presence of the FT-D1^{eh1} C-terminus, whereas Y85 was essential for FT-D1^{eh1} interactions with *Ta*NaKR5 and *Ta*FTIP7 (Figure S5b). These results indicated that the C-terminus

of FT-D1^{eh1}, including Segment B, was essential for its interaction with FDL6, and the Y85 residue was essential for its interactions with TaNaKR5 and TaFTIP7. To further verify these findings, we generated three variants of FT-D1^{eh1}, including FT-D1^{Y85H}, which harbours Tyr85 conversion to His; FT-D1$^{Seg.B}$, carrying a deletion of Segment B (128–141 aa); and FT-D1$^{Y85H\&Seg.B}$, a double mutant harbouring both of the above mutations. As expected, FT-D1^{Y85H} could interact with FDL6, but showed no interaction with TaNaKR5 or TaFTIP7 in yeast cells. Interestingly, both FT-D1$^{Seg.B}$ and FT-D1$^{Y85H\&Seg.B}$ lost the ability to interact with all three proteins (Figure S5c), indicating that Segment B alone is required for FT-D1 molecular interaction. To determine the structural basis of FT-D1 protein interactions, we conducted homology modelling of FT-D1 and its interaction surfaces with 14-3-3A using the structure of Hd3a, which shares 90.3% amino acid identity with FT-D1 (Taoka *et al.*, 2011). The results indicated that surface regions involved in FT-D1-14-3-3A interaction included an acidic lobe at comprising residues D60 and R62 on 14-3-3A and R130 in Segment B of FT-D1^{eh1} spatially isolated from Y85 (Figure 2h,i). These results thus defined the specific residues required for FT-D1^{eh1} interaction with other proteins in early HD.

Both wild-type and mutated *FT-D1* alleles are functional to promote HD and reduce the plant height of wheat

Our analyses indicated that the C-terminus of FT-D1^{eh1} was essential for its protein interactions and early HD phenotype, whereas the effects of regions outside the C-terminus on FT-D1 function remained unknown. Therefore, we selected a homoeologous-conserved target close to the translational start site of *FT1* to perform CRISPR/Cas9-mediated gene editing to knock out the *FT-D1*^{WT} allele in 'Fielder' (Figure S6). Validation of the agroinfiltrated T_0 plants identified four positive transgenic events, including a triple mutant (*ft1-aabbDd*^{KO}), a double mutant (*ft-AD1*^{KO}), and two single mutants (*ft-A1*^{KO} and *ft-D1*^{KO}, Figure 3a). We found that the *ft1-aabbDd*^{KO} plants generated spikes but failed to head throughout the whole developmental stage. The spikelets thus developed abnormally and failed to produce seeds. In addition, internode length was dramatically shorter in the triple mutant compared with Fielder (Figure S7). To verify the gain-of-function in FT-D1^{eh1}, we overexpressed *FT-D1*^{eh1}-flag, driven by the *Ubiquitin* promoter (*FT-D1*^{OE}) in Fielder. Interestingly, spike organogenesis was observed in *FT-D1*^{OE} calluses at the differentiation stage (Figure S8). These callus-grown spikes then degenerated following transfer to soil and emergence of new seedlings. We then screened out three positive OE lines for further analyses by detecting *FT-D1*^{OE}-flag mRNA and protein levels using flag-specific primers and Flag antibody, respectively (Figure S9). Phenotypic comparison between KO and OE plants in field conditions showed that *ft-A1*^{KO}, *ft-D1*^{KO}, and *ft-AD1*^{KO} had HDs 9 days, 5 days, and 11 days later than that of Fielder, respectively, while *FT-D1*^{OE} plants headed approximately 10 days earlier than Fielder (Figure 3b,d). Additionally, spike length was significantly increased by 5.2%, 5.6%, and 8.9% in the *ft-A1*^{KO}, *ft-D1*^{KO}, and *ft-AD1*^{KO} plants, respectively, compared to WT Fielder plants, but decreased by 7.5%–9.5% in *FT-D1*^{OE} lines. We also observed that spikelet number per spike was significantly higher than WT in *ft-AD1*^{KO} plants, but lower in *FT-D1*^{OE} lines, while no significant differences were observed in *ft-A1*^{KO} or *ft-D1*^{KO} plants (Figure 3c,d). We then used scanning electron microscopy (SEM) to observe the morphology of young spikes and found that *ft-D1*^{KO} spikes developed at a relatively slower rate than spikes in Fielder at the floret differentiation stage. Moreover, floret number was increased in *ft-D1*^{KO} plants, and decreased in *FT-D1*^{OE} lines compared with WT controls (Figure 3e). However, the florets exhibited similar morphology at the same developmental stage between *ft-D1*^{KO}, *FT-D1*^{OE}, and Fielder plants (Figure S10). We also observed that plant height significantly increased by 11.0%, 12.6%, and 13.1% in *ft-A1*^{KO}, *ft-D1*^{KO}, and *ft-AD1*^{KO} plants, respectively, while plant height decreased by 6.4%–8.2% in *FT-D1*^{OE} lines compared with Fielder plant height (Figure 3d). To further evaluate the effects of *FT-D1* on the plant height, we compared the peduncle and internode lengths between Fielder and *FT-D1* knockout or overexpression lines and found that the observed differences in plant height were mainly due to variations in the peduncle and fourth internode (Figure 3f,g). Additionally, cytological examination of longitudinal peduncle sections revealed that *FT-D1*^{OE} plants had significantly fewer cells in this region compared to Fielder, while *ft-D1*^{KO} lines had significantly more, suggesting that *FT-D1* reduced plant height by decreasing cell number in stems (Figure 3h,i). These results collectively supported a scenario in which both the *FT-D1*^{eh1} and *FT-D1*^{WT} alleles could exert pleiotropic effects that negatively regulated spike length, spikelet number, and plant height. Moreover, these phenotypic effects were enhanced by the gain-of-function mutation in *FT-D1*^{eh1}, potentially through interactions with 14-3-3A and FDL6 that modulate the expression of various developmental genes.

Identification of the downstream regulation genes of *FT-D1*

To identify genes downstream of *FT-D1* that might contribute to its phenotypic effects, we conducted RNA-seq analysis of young spikes from *ft-D1*^{KO}, *FT-D1*^{OE}, and corresponding WT control plants. On average, 92.4% of the clean reads could be mapped to the Chinese Spring reference genome (IWGSC RefSeq v1.0, Table S2). A total of 3814 (2220 upregulated and 1594 downregulated) and 3341 (1545 upregulated and 1796 downregulated) differentially expressed genes (DEGs) were identified in *ft-D1*^{KO} and *FT-D1*^{OE} lines, respectively (Table S3). Among these DEGs, 1838 genes were identified as common DEGs and showed opposite regulation in *ft-D1*^{KO} and *FT-D1*^{OE} plants (Figure 4a). Gene ontology (GO) analyses of these common DEGs between KO and OE lines were enriched with 66 total significant terms, including 'vegetative meristem growth', 'regulation of circadian rhythm', and 'meristem development' (Figure 4b). To identify hub genes regulated by *FT-D1*, we performed gene co-expression network analysis (WGCNA) based on all DEGs identified in the two comparisons. WGCNA revealed a total of 1925 DEGs across 12 co-expression modules (21–477 genes per module, Figure 4c, Table S4). Among these co-expressed genes, 660 DEGs were identified as hub genes (Table S5). Module-trait association analysis found two modules that were significantly associated with HD (turquoise and midnight blue in Figure 4d, $P < 0.05$), implying that hub genes in these modules might participate in regulating HD. Correlation analysis showed that 75.4% of the hub genes in the turquoise module were highly correlated with HD (GS and MM values >0.8, Figure 4e). Interestingly, we noted that three *ELF5* homoeologs in this module were significantly associated with HD (Table S5), while gene network analysis suggested that *ELF5-2D* might serve as a key hub gene in this module (Figure 4f). These results suggested that *ELF5-2D* could be a hub gene affected by mutation of *FT-D1*. Additionally, exploration of upregulated DEG expression patterns in the *FT-*

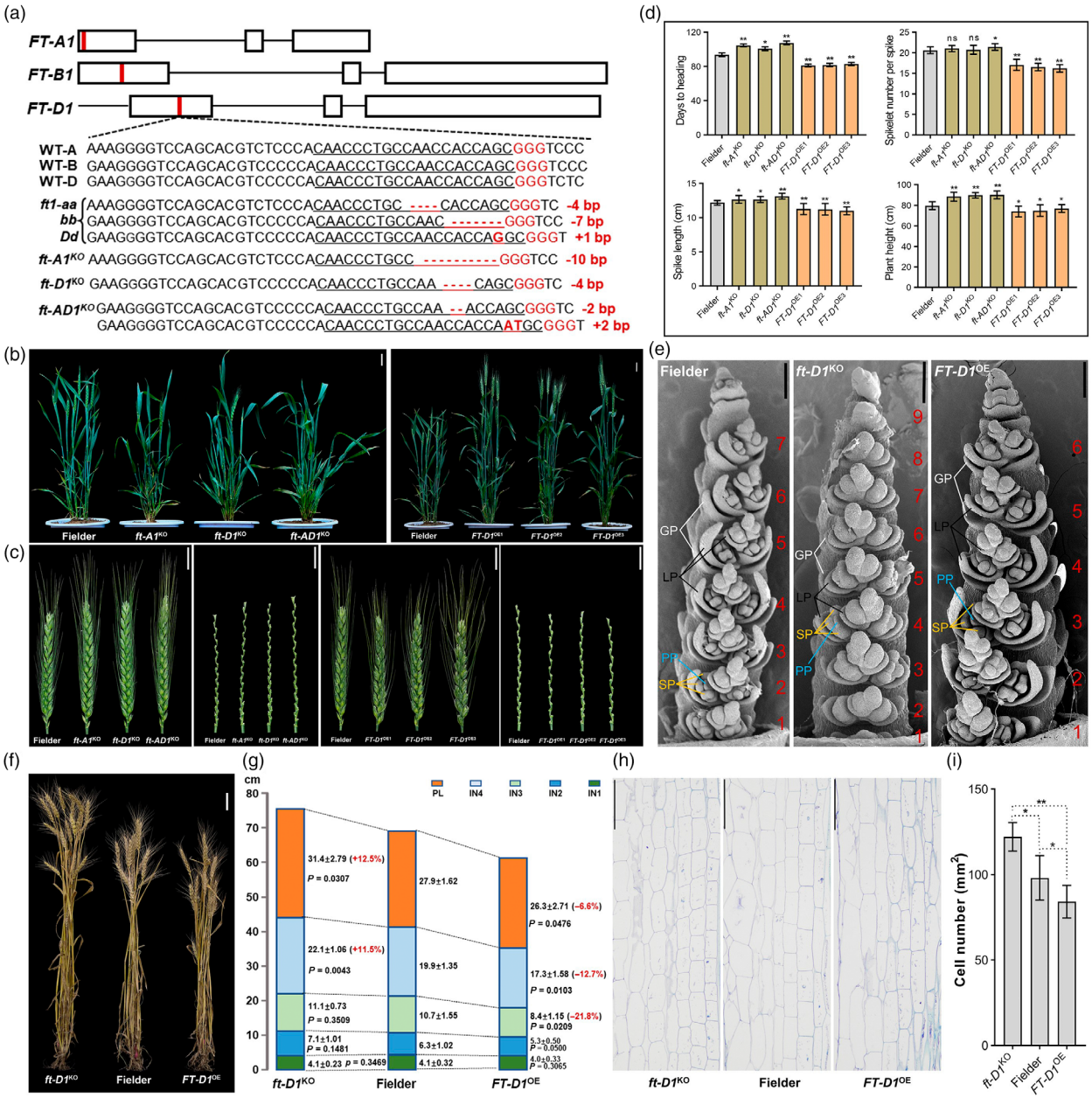

Figure 3 Functional characterization of different *FT-D1* alleles in knockout and overexpression wheat lines. (a) CRISPR/Cas9-mediated gene editing of a conserved target site in *FT1* obtained four mutant plants with different genotypes in the three homoeologues. The triple *ft1* mutant harboured a heterozygous mutation in the D copy and was, therefore, designated as '*ft1-aabbDd*^{KO}'. PAM sequences were highlighted in red and target sequences in homoeologues were underlined. The deletions were indicated by red minus and insertions were highlighted in bold red. (b) Phenotype of the three knockout lines (left) and three overexpression lines (right) at the heading stage. Scale bar = 5 cm. (c) Spike morphology of the three knockout lines and three overexpression lines at the late heading stage. Scale bar = 2 cm. (d) Statistical analyses of HD, plant height, spike length, and spikelet number per spike in the knockout and overexpression wheat lines. Error bars represented mean ± SD; *P* values were determined by two-tailed Student's *t*-test. **P* < 0.05; ***P* < 0.01; ns, no significant difference. (e) SEM observation of the young spikes in *ft-D1*^{KO}, *FT-D1*^{OE}, and corresponding WT plants at the floret differentiation stage. Spikelet was indicated in red numbers. GP, glume primordium; LP, lemma primordium; PP, pistil primordium; SP, stamen primordium; Scale bar = 200 μm. (f) Plant architecture of *ft-D1*^{KO}, *FT-D1*^{OE}, and corresponding WT plants at the maturity stage. Scale bar = 6 cm. (g) Comparison of the peduncle and internodes length in Fielder, *ft-D1*^{KO}, and *FT-D1*^{OE} wheat lines. (h) Cytological observation of the longitudinal section of the peduncles in Fielder, *ft-D1*^{KO}, and *FT-D1*^{OE} wheat lines at the late heading stage. Scale bar = 200 μm. (i) Statistical analysis of cell number in the peduncles of Fielder, *ft-D1*^{KO}, and *FT-D1*^{OE} wheat lines. Data were shown as mean ± SD; *P* values were determined by two-tailed Student's *t*-test. **P* < 0.05; ***P* < 0.01.

D1^{OE} lines and downregulated DEGs in the *ft-D1*^{KO} mutants also identified *ELF5*, as well as other flowering-related genes such as *AGL12* and *FPA* (Figure 4g), further illustrating the regulatory effects of different *FT-D1* alleles. Notably, the flowering-related genes, *VRN1*, *FY*, *HOX14*, and *OFP13*, were only differentially expressed in the *FT-D1*^{OE} lines (Figure 4g). We then validated the transcriptional changes in the six selected genes in young spikes of *ft-A1*^{KO}, *ft-D1*^{KO}, *ft-AD1*^{KO}, and *FT-D1*^{OE} wheat plants by qRT-PCR.

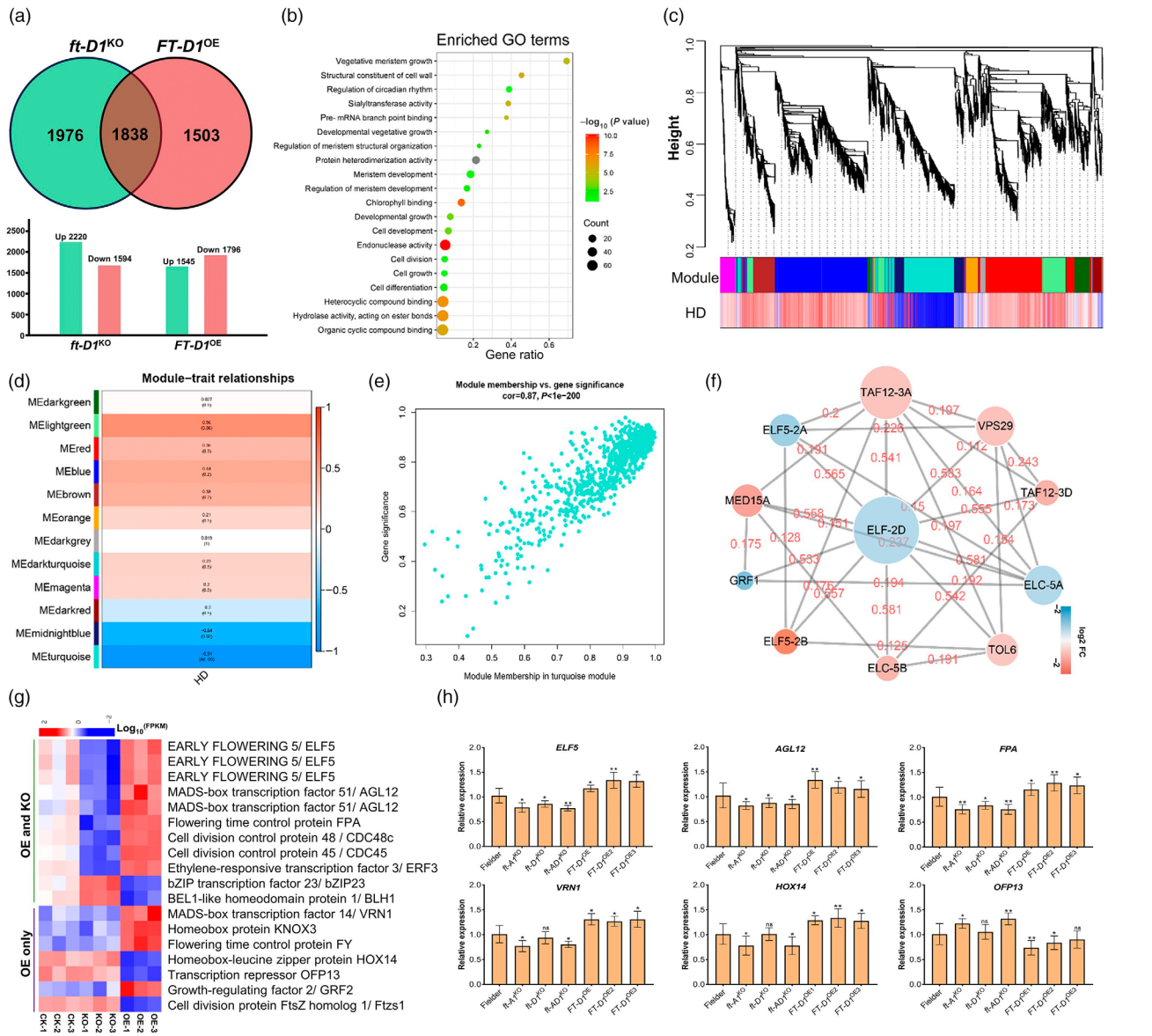

Figure 4 RAN-seq analyses identified *ELF5* as a key gene regulated by *FT-D1*. (a) Venn diagram of the differentially expressed genes (DEGs) in *ft-D1*^{KO} and *FT-D1*^{OE} lines. DEGs were defined as adjusted *P* value <0.05 and $|\log_2 FC| \geq 1$. Each line was analysed with three biological replicates. (b) GO enrichment analyses of DEGs that were contrastingly regulated in *ft-D1*^{KO} and *FT-D1*^{OE}. (c) Hierarchy clustering of co-expression gene modules generated in WGCNA analysis. Different modules were highlighted in different colours. Under the modules, squares with different colours indicated the significance of module-HD association. (d) Association analyses of the 12 modules from WGCNA analysis with HD. Numbers in the bracket and above indicated the *P* and correlation coefficient values, respectively. (e) Correlation of gene significance (GS) and module membership (MM) in the turquoise module. GS indicated the correlation of a given gene with HD. MM represented the correlation of a given gene with the module. (f) The expression weight network of 11 genes indicated *ELF5-2D* was an important hub gene in the turquoise module. (g) Heatmap of selected DEGs from both *ft-D1*^{KO} and *FT-D1*^{OE} lines or only identified from *FT-D1*^{OE} lines. (h) Validation of the 6 selected DEGs by qRT-PCR assays. Data were shown as mean ± SD; $*P < 0.05$; $**P < 0.01$; ns, no significant difference.

(Figure 4h). These results indicated that the *FT-D1*^{WT} and *FT-D1*^{eh1} alleles affected the expression of both shared and exclusive sets of flowering-related genes. Given that *ELF5* genes were identified as potential *FT-D1*-regulated hub genes, we then investigated the expression of *ELF5* in specific tissues using public RNA-seq datasets (http://bar.utoronto.ca/efp_wheat/cgi-bin/efpWeb.cgi). This analysis indicated that *ELF5* is preferentially expressed in the SAM during vegetative growth (Figure S11). Furthermore, we identified a mutant, E783, that harbours a stop-gain mutation in *ELF5-2A*, as well as two mutants, E1315 and E1414, with stop-gain mutations in *ELF5-2B* from a wheat TILLING mutant resource (Xiong *et al.*, 2023) (Figure S12a). In the E783, E1315, and E1414 mutant lines, HD was delayed by 3–5 days compared with that of WT Jing411 under field conditions (Figure S12b). These collective results indicated that *ELF5* may play a role in modulating HD upon regulation by *FT-D1*.

TaNaKR5 and *TaFTIP7* positively regulate HD in wheat

Given the observations that both FT-D1 from the WT and *eh1* mutant interact with TaNaKR5 and TaFTIP7, we next examined their functions in regulating the HD of wheat. To this end, we chose a target site conserved among the three *TaNaKR5* homoeologs for CRISPR/Cas9-mediated knockout in Fielder. A total of 35 T_0 plants with mutations in at least one subgenome copy of *TaNaKR5* were identified. Transgene-free T_3 plants spanning seven different allele combinations at the three *TaNaKR5* subgenome loci were selected for phenotypic analyses (Figure 5a). Under field conditions, assessment of average HD indicated that each individual *nakr5*^{KO} mutant line exhibited delayed HD by 1.8–2.4 days compared to WT controls, while HD was delayed by 3–4 days on average in *nakr5-AB*^{KO}, *nakr5-AD*^{KO}, and *nakr5-BD*^{KO} double mutants, and 5 days in the *nakr5-ABD*^{KO} triple mutant (Figure 5b). Statistical analysis indicated that HD significantly differed between WT plants and the double or triple mutants, but not single mutants. Additionally, plant height was reduced by 11.9% and 21.5% in the *nakr5-AD*^{KO} and *nakr5-ABD*^{KO} lines, respectively, significantly shorter than WT Fielder, but did not reach significance in other mutants (Figure 5c). These results suggested that *TaNaKR5-A* and *TaNaKR5-D* like function redundantly in regulating the plant height. Moreover, spike length was significantly shortened by 7.6% and 8.5% in the *nakr5-AD*^{KO} and *nakr5-ABD*^{KO} lines, respectively, in comparison with Fielder (Figure 5d). However, only the *nakr5-ABD*^{KO} triple mutant had significantly fewer spikelets per spike compared to Fielder controls (Figure 5e). These results indicated that *TaNaKR5* finely regulates HD, plant height, and spike morphology. Following a similar strategy, we induced frameshift mutations by gene editing at a conserved site in the three *TaFTIP7* subgenome homoeologs that altered ~97% of their respective amino acid sequences. We then screened out positive transgenic events and selected four T_0 plants, including single mutations in either the A or D copies; double mutation of both the A and D copies; and a triple mutant with disruption of all three copies (Figure 5f). The positive transgenic lines were self-pollinated for two generations and the transgene-free T_3 plants were selected for phenotypic analyses. Phenotypic analyses of *ftip7*^{KO} mutants showed slight, albeit non-significant differences in HD among the *ftip7-A*^{KO} and *ftip7-D*^{KO}, while *ftip7-AD*^{KO} and *ftip7-ABD*^{KO} mutants had HD significantly delayed by an average of 4.1 and 5.3 days, respectively, compared with Fielder (Figure 5g). In addition, spike length was significantly increased by 7.6% only in the *ftip7-ABD*^{KO} triple mutant (Figure 5h). Further investigation showed that all *ftip7*^{KO} mutants displayed plant height and spike number per spike similar to Fielder (Figure 5i). These collective results suggested that *TaNaKR5* and *TaFTIP7* are involved in the regulation of HD, and *TaNaKR5* homoeologs act redundantly on plant height and spike length in wheat.

Transcriptional and translational relation of *FT-D1* with its interactor genes

To investigate the subcellular localization of FT-D1 and its interaction partners, we fused them with a green fluorescent protein (GFP) reporter and transiently expressed them in wheat protoplasts. Fluorescence microscopy revealed the presence of FT-D1-GFP signal in both the nucleus and cytoplasm, while FDL6-GFP fluorescence was exclusively detected in the nucleus, and 14-3-3A-GFP was observed in the nucleus and cytoplasm (Figure 6a). These results were consistent with our above BiFC assays that showed FT-D1 could interact with FDL6 in the nucleus, and with 14-3-3A in both the nucleus and cytoplasm. Similar to their orthologues in *Arabidopsis* and rice, TaNaKR5-GFP and TaFTIP7-GFP signals were localized in the endoplasmic reticulum, suggesting that their functions may be conserved among plant species (Figure 6a). To define the tissue-specific patterns of expression in these FT-D1 interactors, we conducted qRT-PCR assays in five different tissues at the heading stage. These assays indicated that *FDL6*, *TaNaKR5*, and *TaFTIP7* were mainly expressed in leaf tissues. By contrast, *14-3-3A* transcripts were predominantly detected in spikes (Figure 6b). Based on this spatial distribution of expression, we focused on the expression of *FT-D1* and its interaction partners in leaves or spikes of different transgenic mutants. In the four *ftip7*^{KO} lines, both *FT-D1* and *FDL6* were significantly downregulated in leaf tissues of *ftip7-AD*^{KO} and *ftip7-ABD*^{KO} plants, but not in the two single mutants, while *TaNaKR5* and *14-3-3A* expression were not significantly affected (Figure 6c). Further analysis of the seven *nakr5*^{KO} mutant lines suggested that *TaFTIP7*, 14-3-3A, and FDL6 were expressed at comparable levels in leaves, whereas *FT-D1* transcription was significant in all mutants except *nakr5-B*^{KO} (Figure 6d). As *FT1* mainly functions in the SAM, we evaluated the expression of FT-D1 interaction partners in the young spikes of *FT1* KO and *FT-D1* OE lines. The results showed that *TaNaKR5* and *TaFTIP7* expressions were not significantly affected in the *ft-A1*^{KO}, *ft-D1*^{KO}, *ft-AD1*^{KO}, or OE lines, but FDL6 and 14-3-3A expression significantly decreased in the *ft-AD1*^{KO} mutant and increased in the OE lines (Figure 6e). To further explore how *TaNaKR5* and *TaFTIP7* regulate HD, we measured FT-D1 protein levels in the leaves and young spikes of *nakr5*^{KO} and *ftip7*^{KO} mutants and found that FT-D1 protein accumulated in the flag leaves of the seven *nakr5*^{KO} mutants at comparable levels to that in Fielder. However, FT-D1 protein abundance was significantly reduced in young spikes of the *nakr5*^{KO} double and triple mutant lines (Figure 6f and Figure S13a,c). Likewise, FT-D1 abundance was significantly decreased in spikes of the double and triple *ftip7*^{KO} lines compared with Fielder, while FT-D1 protein levels in leaf tissues were similar across these mutants (Figure 6g and Figure S13b,d). These results indicated that both *TaNaKR5* and *TaFTIP7* are important to FT-D1 accumulation in wheat spikes. Based on these findings, we presented a working model of different *FT-D1*^{WT} and *FT-D1*^{eh1} actions on HD regulation (Figure 7). In this model, both FT-D1 proteins from the *eh1* and WT were expressed in leaves and then transported to the SAM with the assistance of TaNaKR5 and TaFTIP7. In SAM, FT-D1^{eh1} could interact with 14-3-3A and FDL6 to form the FAC and thereby enhancing the transcriptional regulation of target genes; whereas FT-D1^{WT} lost the ability to form the FAC with 14-3-3A and FDL6 and exhibited a delayed HD. As FT-D^{WT} was also partially functional to affect HD, we inferred that FT-D1 could interact with other undetermined TFs in a C-terminus-independent manner to modulate the transcription of downstream genes such as *ELF5*.

Discussion

Here, through map-based cloning, we identified a C-terminal gain-of-function mutation in *FT-D1* that accelerates HD, while decreasing plant height and spike length in the *eh1* γ-ray wheat mutant. Similarly, single nucleotide insertion/deletion variants in *FT-D1* exon 3 associated with HD and spikelet number have been widely detected in wheat accessions from diverse geographical

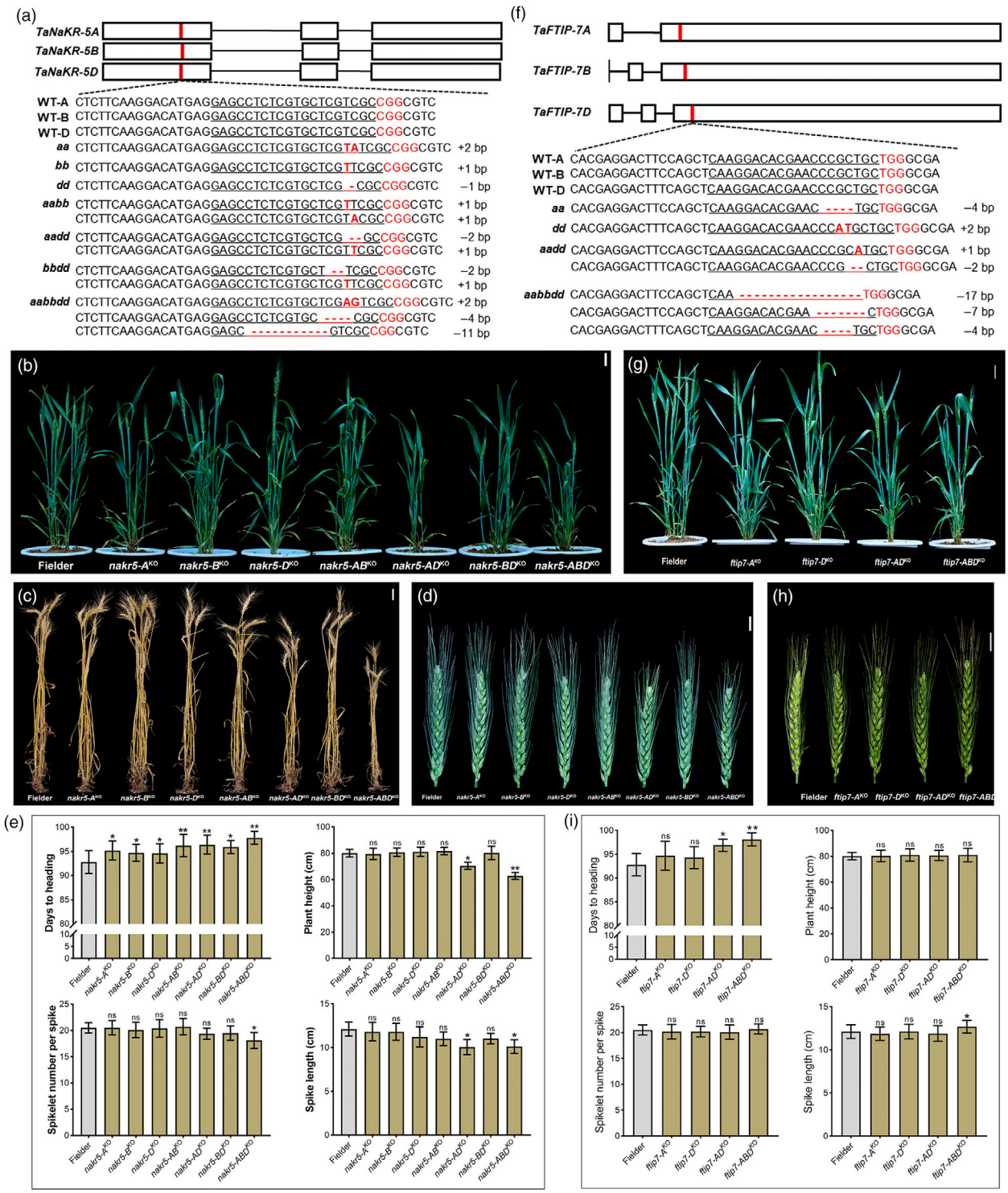

Figure 5 Functional characterization of *TaNaKR5* and *TaFTIP7* in CRISPR/Cas9-mediated knockout wheat lines. (a) Mutant identification of positive *nakr5*^{KO} lines generated by gene editing assays. The homoeologous-conserved target sequences in *TaNaKR5* were indicated by red lines and the target sequences were underlined. PAM sequences were highlighted in red. The deletions were indicated by red minus, and insertions were highlighted in bold red. Phenotypes of the seven *nakr5*^{KO} mutant plants at the heading stage (b) and maturity stage (c). Scale bar = 5 cm. (d) Spike morphology of the seven *nakr5*^{KO} plants at the late heading stage. Scale bar = 2 cm. (e) Statistical analysis of the HD, plant height, spike length, and spikelet number per spike in the seven *nakr5*^{KO} mutant lines. (f) Mutant identification of positive *ftip7*^{KO} mutants generated by gene editing assays. (g) Phenotypes of the four *ftip7*^{KO} mutant plants at the heading stage, Scale bar = 5 cm. (h) Spike morphology of the four *ftip7*^{KO} mutant lines at the late heading stage. Scale bar = 2 cm. (i) Statistical analysis of HD, plant height, spike length, and spikelet number per spike in the four *ftip7*^{KO} mutant plants. Error bars represented the mean ± SD; *P* values were determined by two-tailed Student's *t*-test. **P* < 0.05; ***P* < 0.01; ns, no significant difference.

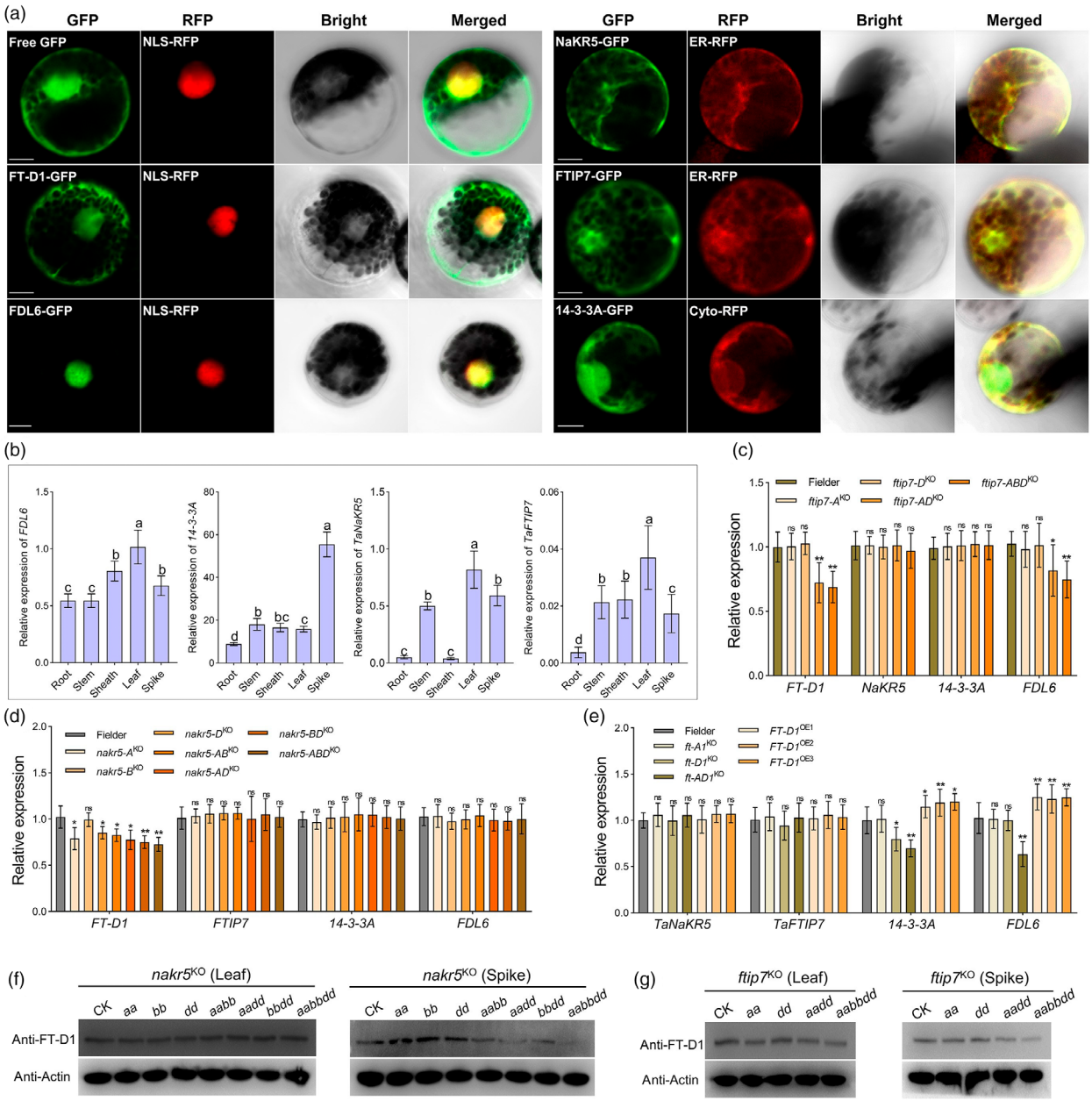

Figure 6 Molecular characterization of FT-D1 and its four interacting partners. (a) Transient expression of GFP-tagged FT-D1, FDL6, TaNaKR5, TaFTIP7, and 14-3-3A proteins driven by the CaMV 35S promoter in wheat protoplasts. After 16 h of transformation, wheat protoplasts were observed using a confocal microscope. Scale bar = 5 μm. (b) Tissue-specific expression patterns of *FDL6*, *TaNaKR5*, *TaFTIP7*, and *14-3-3A* in Fielder at the heading stage. Expression levels were normalized to the wheat *Actin* gene. Error bars indicate the mean ± SD. Different letters indicate significant differences at $P < 0.05$. (c) Relative expression of *FT-D1*, *TaNaKR5*, *14-3-3A*, and *FDL6* in the leaves of the four *ftip7*^{KO} mutants at the heading stage. (d) Relative expression of *FT-D1*, *TaFTIP7*, *14-3-3A*, and *FDL6* in the leaves of the seven *nakr5*^{KO} mutants at the heading stage. (e) Relative expression of *TaNaKR5*, *TaFTIP7*, *14-3-3A*, and *FDL6* in the spikes of the *FT1* knockout and *FT-D1* overexpression lines at the heading stage. Error bars indicate the mean ± SD; *$P < 0.05$; **$P < 0.01$; ns, no significant difference. Protein accumulation of FT-D1 in the leaves and spikes of the seven *nakr5*^{KO} mutants (f) and the four *ftip7*^{KO} mutants (g) at the floret differentiation stage. FT-D1 was detected by FT-D1 antibodies generated in this study. Wheat Actin gene was used as endogenous control.

origins (Bonnin *et al.*, 2007; Chen *et al.*, 2022). However, the mechanism through which this frameshift variation can promote earlier HD has remained unknown. Our extensive protein interaction analyses revealed that the frameshift in *FT-D1*^{eh1} resulted in competence to interact with the 14-3-3A and FDL6 proteins, and consequently, the formation of the FAC. In turn, the FAC could modulate the expression of flowering-related genes, resulting in early heading in *eh1* plants. Consistent with these findings, ectopic expression of exon 4 from the C-terminal region of *AcFT* has been shown to partially compensate for the *ft-1* late-flowering phenotype in *Arabidopsis* (Hou and Yang, 2016). Additionally, in our current study, knockout of the *FT-D1*^{WT} allele, which cannot interact with 14-3-3A and FDL6 to form the FAC, caused late heading, supporting that *FT-D1* functions in accelerating HD and decreasing plant height are partially independent of the C-terminus binding activity of the *eh1*

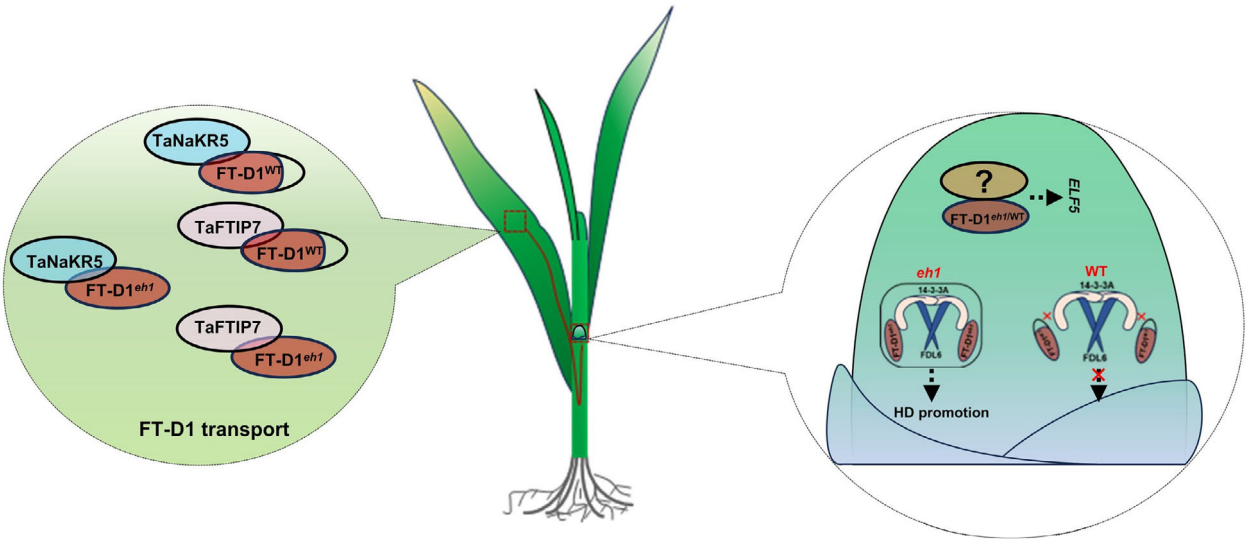

Figure 7 A putative model depicting how the gain-of-function mutation in FT-D1eh1 promoted HD in wheat.

mutant. Aligning well with this scenario, *Brassica rapa* reportedly harbours a variety of FT-like proteins with the C-terminus divided FD-interacting and FD-independent regions, both of which are functional to regulate flowering (Lee *et al*., 2023). In addition to interacting with FAC components, several FT-interacting TFs (*e.g*. TCP family members) that participate in plant development have also been previously identified (Mimida *et al*., 2011; Niwa *et al*., 2013). It is, therefore, reasonable to speculate that the *FT-D1*^{WT} allele may interact with other TFs to promote heading. Interestingly, the single nucleotide insertion in *FT-D1* of *eh1* mutant is identical to the ancestral *FT-D1*(G) allele, which is prevalently distributed in hexaploid wheat and *Aegilops tauschii* (Chen *et al*., 2022). Consistently, the previous studies have indicated that artificial mutagenesis could induce reverse mutation in plant species (Chen *et al*., 2024; Sun *et al*., 2023). An analysis of the SNPs and Indels identified by exome-capturing sequencing found that the mutation numbers in the *eh1* are similar to the average number of mutations based on a large-scale wheat mutant resource (Table S6; Xiong *et al*., 2023). These findings collectively indicated that the mutation occurred in *FT-D1*^{eh1} was resulted from γ-ray mutagenesis but not background contamination.

Although the functions of *FT-D1* and its orthologues in cereal crops have been discussed in several studies (Chen *et al*., 2022; Shaw *et al*., 2019; Zhu *et al*., 2017), a comprehensive, in-depth, mechanistic investigation of its activity is necessary to understand and apply its pleiotropic effects in breeding. Here, we show that wheat *FT1* homoeologs exhibit variation in the strength of their pleiotropic interactions and act redundantly in determining HD, similar to the three copies of the vernalization gene, *VRN1*, among which *VRN-A1* exhibits the strongest effects on HD while *VRN-D1* exerts the weakest effects (Dubcovsky *et al*., 2006; Zhang *et al*., 2008). In crops, HD and plant height are often tightly linked. For example, the key HD determinants, *Ghd8* (Yan *et al*., 2011), *Ghd7.1* (Liu *et al*., 2013), and *Hd1* (Yan *et al*., 2012), also affect plant height, and the phenotypic effects of *Rth25* on plant height are accompanied by changes in HD (Mo *et al*., 2018). In the triple *ft1-aabbDd*^{KO} mutant, stem elongation is severely restricted and plants fail to complete heading, suggesting that *FT1* could be a potential target to simultaneously improve the plant height and adaptation in wheat breeding. Identifying the downstream target genes of *FT1* will help to further uncover its multifaceted roles in wheat development.

Our results indicate that flowering regulator genes such as *ELF5*, *AGL12* (*MADS-box 51*), *FPA*, *FY*, and *VRN1* serve as direct or indirect downstream targets of *FT-D1*. Moreover, WGCNA revealed a core regulatory role of *ELF5* in *FT-D1* transgenic plants. In wheat, the *ELF5* paralog, *ELF3*, is critical for photoperiodic regulation of HD via binding to regulatory sites in *Ppd1* (Köhler *et al*., 2023; Zikhali *et al*., 2016). In addition, mutations in the *Arabidopsis* mutant, *elf5*, partially suppress flowering signals in the photoperiod response pathway, consequently inducing early flowering (Noh *et al*., 2004). These findings support a possible role of *ELF5* in *FT-D1*-mediated photoperiodic regulation of HD. RNA-seq analysis also identified differential regulation of several pathways and genes involved in controlling cell division and growth, such as *CDC45*, *CDC48*, and *Ftzs1* (Figure 4). The aberrant expression of these genes in the *FT-D1* transgenic mutants suggests their participation in *FT-D1*-mediated regulation of the plant height, aligning well with our findings of significantly altered cell number in the stems of *FT-D1* transgenic wheat plants (Figure 3). Indeed, overexpression of the *JcFT* gene has been reported to significantly decrease plant height due to reduced cell number in tobacco stems (Wu *et al*., 2022b). However, it remains largely unknown how FT-D1 interacts with other regulatory genes to modulate cell division and growth in wheat stems.

To investigate the mechanisms through which FT-D1 interacts with other flowering genes, we referred to previous studies that revealed the Y85H residue conversion or divergence in the 'Segment B' external loop confers antagonistic activity on floral regulation between FT and TFL1, a close paralog of FT (Ahn *et al*., 2006; Hanzawa *et al*., 2005). Our results show that the Y85H substitution in FT-D1^{eh1} disrupts its interactions with TaNaKR5 and TaFTIP7, but not with FDL6 (Figure S6), which is consistent with structural analysis that showed this residue is spatially isolated from the FT-D1–14-3-3A binding surfaces (Figure 2). Additionally, disrupting the conserved Segment B external loop in FT-D1^{eh1} was sufficient to abolish its interactions with all tested proteins, indicating that Segment B is necessary for FT-D1 protein interactions with different partners. Indeed, the

Segment B conformation has been previously demonstrated to play a critical role in FAC formation and flowering regulation, potentially via the recruitment of transcriptional coactivators (Nakamura *et al*., 2019; Taoka *et al*., 2011). Our interaction analyses support the likelihood that these functionally conserved sites in FT-D1 mediate its specific binding activity with different transcriptional regulators, which together affect wheat flowering time and cell development. Further investigation is still necessary to determine whether the contrasting regulatory effects of Y85H and divergent Segment B on HD are conserved in wheat.

In *Arabidopsis*, *NaKR1* encodes an ion transporter in phloem that regulates flowering time by mediating the long-distance delivery of FT from sieve elements to the SAM via phloem sap (Tian *et al*., 2010; Zhu *et al*., 2016). In conjunction with NaKR1, the multiple C2 domain and transmembrane region protein, FTIP1, is required for FT translocation from companion cells to sieve elements (Liu *et al*., 2012). In this study, we show that the wheat orthologues of both NaKR1 and FTIP1, TaNaKR5 and TaFTIP7, exert gene dosage effects on HD regulation, potentially due to variability in the activity of different subgenome copies. Additionally, our results suggest that *TaNaKR5* can influence plant height and spike length independent of changes in FT-D1 transcription or protein accumulation, as individual knockouts of *TaNaKR5* or *FT-D1* resulted in opposite plant height and spike length phenotypes in wheat. Our findings of FT-D1 interaction with TaNaKR5 and TaFTIP7, along with their localization to the endoplasmic reticulum, and the reduced FT-D1 accumulation in spikes but not leaves of *nakr5* and *ftip7* knockout mutants suggest their possible roles in long-distance transport of FT-D1 in wheat. Although these experimental findings in this study indirectly support the roles of TaNaKR5 and TaFTIP7 in FT-D1 translocation, specific biochemical and molecular evidences are still needed to further substantiate the functions of TaNaKR5 and TaFTIP7 in the FT-D1-meidated flowering regulation.

Conclusion

In this study, we used BSA and map-based cloning to identify a gain-of-function mutation in the C-terminus of *FT-D1* that exerts pleiotropic effects on the HD, plant height, and spike length in the *eh1* γ-ray-induced wheat mutant. This frameshift mutation resulted in *FT-D1* acquiring the ability to interact with 14-3-3A and FDL6 and subsequently form the FAC, in turn altering the transcriptional regulation of flowering-related genes in the *eh1* mutant. This mutation in *FT-D1* had no obvious effect on its interactions with TaNaKR5 or TaFTIP7, both of which retained their respective functions in determining HD, potentially by mediating long-distance translocation of FT-D1. Furthermore, exogenous expression of different FT-D1 variants showed that both the WT and *eh1* mutant alleles functionally regulated HD and plant height. Finally, we identified *ELF5* as a core regulator of HD and a potential downstream target of FT-D1. These results enhance our understanding of the pleiotropic effects and regulatory functions of FT-D1, while also providing valuable genetic resources for wheat improvement.

Materials and methods

Plant materials and growth conditions

The *early heading 1* (*eh1*) wheat mutant was mutated by γ-ray irradiation using wheat line Zhongyuan9 as wild type (WT) (Li *et al*., 2020). The *eh1* mutant was crossed with WT to develop an F_2 population containing 1081 plants for gene mapping. Parent and F_2 plants were grown at the Zhongpuchang Experimental Station of the Institute of Crop Sciences, Chinese Academy of Agricultural Sciences (Beijing, China) from October to June during 2019–2020 for phenotypic assessments.

Bulked segregant analysis

For BSA, a total of 72 early and 84 late heading plants from the F_2 population were selected and evenly divided into two replicates. DNA bulks were subjected to whole exome sequencing using the Illumina NovaSeq 6000 platform (Bioacme Biotech., Wuhan, China). Raw sequencing data were filtered with Fastp software (https://github.com/OpenGene/fastp) to generate clean reads and then were aligned to the IWGSC RefSeq v1.0 to call variations. The Euclidean distance (ED) for each SNP was calculated and the ED^4 values were fitted using a local weighted regression algorithm to eliminate background noise (Hill *et al*., 2013).

QTL mapping

SNPs from two parent lines were selected to convert KASP markers using the online primer design pipeline Polymarker (Ramirez-Gonzalez *et al*., 2015). PCR reactions for KASP genotyping were conducted as previously described (Li *et al*., 2023). Fluorescence signals were captured with the FLUOstar Omega reader (BMG LABTECH, Offenburg, Germany), and genotype discrimination was conducted with the Klustercaller software (LGC Genomics, London, UK). The linkage map was constructed using the MAP function of IciMapping 4.1 (Meng *et al*., 2015). QTL mapping was performed using an inclusive composite interval mapping algorithm in IciMapping 4.1 with default parameters. Primer sequences are listed in Table S7.

Yeast two-hybrid (Y2H) assay

The coding sequences (CDS) of *FT-D1*^{eh1} and *FT-D1*^{WT} were amplified from the leaf cDNA samples in *eh1* and WT, and then cloned into the pGBKT7 plasmid. The CDS of *FDL2*, *FDL6*, and *14-3-3A* were amplified from WT using previously developed primers (Li *et al*., 2015; Li and Dubcovsky, 2008). *TaNaKR3*, *TaNaKR5*, *TaFTIP5*, and *TaFTIP7* were identified by Blastn search using *NaKR1* (*AT5G02600*) and *FTIP1* (*AT5G06850*) as queries, respectively. These CDS were cloned into the pGADKT7 plasmid using a ClonExpress MultiS One-Step Cloning Kit (Vazyme, Nanjing, China). The bait-BD and AD-prey vectors were co-transformed into the Y2H-gold yeast strains and grown on the SD/−Trp/−Leu/-His/−Ade selective medium. PCR primers are listed in Table S7.

GST pull-down assay

To express GST-tagged proteins, the full-length CDS of *FT-D1*^{eh1}, *FT-D1*^{WT}, and *14-3-3A* were cloned into the vector pGEX-4T-1. The CDS of *FDL6*, *TaNaKR5*, *14-3-3A*, and truncated *TaFTIP7* with the transmembrane domain deprived were cloned into the vector pMAL-c6T to generate MBP-tagged proteins (Table S7). All recombinant vectors were transformed into *Escherichia coli* BL21 (DE3) to express fusion proteins. The GST-tagged proteins were extracted and immobilized using GST mag-beads (Sangon Biotech., Shanghai, China). The MBP-tagged proteins were incubated with GST fusion proteins overnight at room temperature. Proteins retained on the beads were determined by Western blot analyses using anti-GST (AG768; Beyotime Biotech., Shanghai, China) and anti-MBP (E-AB-20013; Elabscience Biotech., Wuhan, China).

Luciferase complementation imaging (LCI) and bimolecular fluorescence complementation (BiFC) assays

The CDS of *FT-D1*^{eh1}, *FT-D1*^{WT}, and *14-3-3A* were cloned into vectors p1300-35S-cLuc and pSAT4A-cEYFP-N1 to generate the cLuc- and cYFP-tagged fusion proteins, respectively. The CDS of *FDL6*, *TaNaKR5*, *TaFTIP7*, and *14-3-3A* were cloned into vectors p1300-35S-nLuc and pSAT4A-nEYFP-C1 to express the nLuc- and nYFP-tagged fusion proteins, respectively (Table S7). The nLuc and cLuc fused vectors, and the nYFP- and cYFP-fused vectors were transformed into *Agrobacterium* strain GV3101 and subsequently infiltrated into 6-week-old tobacco leaves for LCI and BiFC assays, respectively. BiFC signals were observed using a laser confocal microscope (Zeiss LSM 770, Oberkochen, Germany).

Homology modelling and molecular docking

The amino acid sequences of FT-D1 were submitted to the Swiss Model (https://swissmodel.expasy.org/) for homology modelling. The 3D structure of FT-D1 was analysed using the rice Hd3a as a template. The structure of the FT-D1-14-3-3A complex was determined by PyMOL (http://www.pymol.org/) using the rice FAC complex as a template (Taoka *et al*., 2011).

Gene editing and plant transformation

CRISPR/Cas9-mediated gene editing was performed on *TaFT1*, *TaNaKR5*, and *TaFTIP7*. Three conserved targets for *TaFT1*, *TaNaKR5*, and *TaFTIP7* were selected as the single-guide (sg) RNA sequences that were driven by the *TaU3* promoter, respectively. These sgRNA were cloned into the pWMB110 vector that harboured a *Bar* gene as a selection marker. The immature wheat embryos from Fielder were transformed with the pWMB110 vector using *Agrobacterium*-mediated transformation. Gene-specific primers used in the mutation identification are listed in Table S7. To generate FT-D1^{eh1} overexpression lines, the CDS of *FT-D1*^{eh1} was fused with the flag and cloned into an entry vector pDONR207, and then transferred to a destination vector pUbiGW according to the handbook of Gateway cloning (Invitrogen, Carlsbad, CA). The recombinant vector was transformed into the immature embryos of Fielder using the *Agrobacterium*-mediated method (Ishida *et al*., 2015).

SEM analysis

The young spikes from Fielder, *ft-D1*^{KO}, and *FT-D1*^{OE} were collected at the floret differentiation stage and then were vacuum fixed with 2% glutaraldehyde in phosphate buffer, followed by dehydration with a standard series of ethanol with gradient concentrations, and critical point-dried in liquid CO_2. The dehydrated tissues were coated with platinum using an ion spatter. Photos were taken using a scanning electron microscope (SEM3200; CIQTEK, Hefei, China).

Sub-cellular localization

The CDS of *FT-D1*, *FDL6*, *TaNaKR5*, *TaFTIP7*, and *14-3-3A* were cloned into the expression vector pAN580-GFP at the *BglII* and *PstI* sites (Table S7), respectively. The resultant vectors were transformed into wheat protoplast as previously described (Xiong *et al*., 2022). After overnight incubation at room temperature, GFP signals were observed with a laser confocal microscope (Zeiss LSM 880, Oberkochen, Germany). The cytoplasm- and nucleus-localized mCherry markers were used as previously described (Ma *et al*., 2019; Xiong *et al*., 2022). The pCAMBIA1300-35S-E.R-mCherry-HDEL plasmid (ZK7122; Zoman Biotech., Beijing, China) was used as a endoplasmic reticulum-localized mCherry marker.

Quantitative real-time PCR (qRT-PCR)

Total RNA was extracted with TRIzol reagent (Sigma-Aldrich, Saint Louis, USA) and the first-strand cDNA was synthesized using the Goldenstar® RT6 cDNA synthesis kit (Tsingke Biotech., Beijing, China). The qRT-PCR reaction was conducted using ChamQ SYBR qPCR master mix (Vazyme, Nanjing, China) according to the manufacturer's instructions. Relative expressions were normalized to a wheat *Actin* gene using the $2^{-\triangle\triangle CT}$ method (Livak and Schmittgen, 2001). Primers used for qRT-PCR analyses are listed in Table S7.

FT-D1 protein determination

For determining FT-D1 proteins, total proteins were extracted from flag leaves and young spikes at the floret differentiation stage from *nakr5* and *ftip7* KO mutants. Briefly, 10 μg of total protein was used for Western blot (WB) analysis with the newly generated FT-D1 antibody (1:1000) in this study (Abmart, Shanghai, China). The primary FT-D1 antibody was then recognized by the HRP-labelled goat anti-mouse IgG (1:5000, cat: A0216; Beyotime, Shanghai, China). Chemiluminescent was detected with an enhanced ECL kit (cat: E411-04; Vazyme, Nanjing, China), and images were acquired using the Tanon 5200 imaging system (Tanon Biotech., Shanghai, China). Three biological replicates were used for each *nakr5* and *ftip7* genotype in WB analysis. Relative intensity of WB bands was analysed using the ImageJ software (http://imagej.en.softonic.com/).

RNA-seq and data process

Samples used for RNA-seq analysis were collected from young spikes of Fielder, *ft-D1*^{KO}, and *FT-D1*^{OE} at the floret differentiation stage. Total RNA was extracted with TRIzol reagent, and the quality and quantity were determined using a NanoDrop ND-2000 Spectrophotometer (Thermo Scientific, Carlsbad, CA, USA). RNA-seq libraries were constructed according to the Illumina manufacturer's recommendations and high-throughput sequencing was performed in the Illumina NovaSeq6000 platform. Raw sequencing data were filtered by the fastp software (https://github.com/OpenGene/fastp) to generate clean reads that were then aligned to the IWGSC RefSeq v1.0 using HISAT software (Kim *et al*., 2015) with default parameters. Transcript levels were determined using StringTie (Pertea *et al*., 2015) and normalized with the FPKM (fragments per kilobase of transcript per million mapped reads) algorithm (Trapnell *et al*., 2010). DEGs in different samples were identified using the DESeq2 R packages and defined as adjusted P value <0.05 and $|\log_2 FC| \geq 1$.

Weighted gene co-expression network analysis (WGCNA)

The DEGs identified from *ft-D1*^{KO} and *FT-D1*^{OE} transgenic lines were used to perform WGCNA with the R package (Langfelder and Horvath, 2008). Briefly, a hierarchical cluster tree was constructed based on the gene expression correlation adjacency matrix that was determined by the soft threshold. The minimal module size and soft threshold value were set to 20 and 9 as determined by the scale-free topology, respectively. The module-HD correlation was evaluated by Pearson's correlation coefficient. Gene significance and module membership for each gene in the

key module were calculated to determine their associations with HD. Visualization of gene networks was conducted by Cytoscape software (Shannon *et al*., 2003).

Acknowledgements

We thank Dr. Ke Wang (Institute of Crop Sciences, Chinese Academy of Agricultural Sciences) for technical assistance in wheat transformation. This work was supported by the National Key Research and Development Program of China (Grant No. 2022YFD1200700), the National Natural Science Foundation of China (Grant No. 32172040), the Nuclear energy development research programme of the State Administration of Science, Technology, and Industry for National Defense (Crop Varietal Improvement and Insect Pests Control by Nuclear Radiation), the China Agriculture Research System of MOF and MARA (Grant No. CARS-03), and the Innovation Program of Chinese Academy of Agricultural Sciences.

Conflict of interest

The authors declare no conflict of interest.

Author contributions

Conceptualization, LL; formal analysis YL, HX, and HG; methodology: YL, HX, YX, LZ, JG, and HL; resources: SZ, YD, CZ, and ZF; Writing – original draft: YL and HX; Writing – review & editing: LL; supervision: LL; funding acquisition: LL. All authors have read and approved the final version of the manuscript.

Data availability statement

The data that support the findings of this study are openly available in the National Center for Biotechnology Information BioProject database at https://www.ncbi.nlm.nih.gov/search/all/?term=PRJNA1050381, reference number PRJNA1050381.

References

Abe, M., Kobayashi, Y., Yamamoto, S., Daimon, Y., Yamaguchi, A., Ikeda, Y., Ichinoki, H. *et al*. (2005) FD, a bZIP protein mediating signals from the floral pathway integrator FT at the shoot apex. *Science* **309**, 1052–1062.

Ahn, J.H., Miller, D., Winter, V.J., Banfield, M.J., Lee, J.H., Yoo, S.Y., Henz, S.R. *et al*. (2006) A divergent external loop confers antagonistic activity on floral regulators FT and TFL1. *EMBO J.* **25**, 605–614.

Beales, J., Turner, A., GriYths, S., Snape, J.W. and Laurie, D.A. (2007) A *Pseudo-Response Regulator* is misexpressed in the photoperiod insensitive *Ppd-D1a* mutant of wheat (*Triticum aestivum* L.). *Theor. Appl. Genet.* **115**, 721–733.

Bonnin, I., Rousset, M., Madur, D., Sourdille, P., Dupuits, C., Brunel, D. and Goldringer, I. (2007) FT genome A and D polymorphisms are associated with the variation of earliness components in hexaploid wheat. *Theor. Appl. Genet.* **116**, 383–394.

Chen, X., Xiong, H., Guo, H., Chen, S., Zhao, L., Xie, Y., Gu, J. *et al*. (2024) Mapping and identification of a reverse mutation of Rht2 that enhances plant height and thousand grain weight in an elite wheat mutant induced by spaceflight. *Plant Physiol. Biochem.* **207**, 108425.

Chen, Z., Ke, W., He, F., Chai, L., Cheng, X., Xu, H., Wang, X. *et al*. (2022) A single nucleotide deletion in the third exon of *FT-D1* increases the spikelet number and delays heading date in wheat (*Triticum aestivum* L.). *Plant Biotechnol. J.* **20**, 920–933.

Corbesier, L., Vincent, C., Jang, S., Fornara, F., Fan, Q., Searle, I., Giakountis, A. *et al*. (2007) FT protein movement contributes to long-distance signaling in floral induction of *Arabidopsis*. *Science* **316**, 1030–1033.

Distelfeld, A., Li, C. and Dubcovsky, J. (2009a) Regulation of flowering in temperate cereals. *Curr. Opin. Plant Biol.* **12**, 178–184.

Distelfeld, A., Tranquilli, G., Li, C., Yan, L. and Dubcovsky, J. (2009b) Genetic and molecular characterization of the *VRN2* loci in tetraploid wheat. *Plant Physiol.* **149**, 245–257.

Dubcovsky, J. and Dvorak, J. (2007) Genome plasticity a key factor in the success of polyploid wheat under domestication. *Science* **316**, 1862–1865.

Dubcovsky, J., Lijavetzky, D., Appendino, L. and Tranquilli, G. (1998) Comparative RFLP mapping of *Triticum monococcum* genes controlling vernalization requirement. *Theor. Appl. Genet.* **97**, 968–975.

Dubcovsky, J., Loukoianov, A., Fu, D., Valarik, M., Sanchez, A. and Yan, L. (2006) Effect of photoperiod on the regulation of wheat vernalization genes *VRN1* and *VRN2*. *Plant Mol. Biol.* **60**, 469–480.

Giakountis, A. and Coupland, G. (2008) Phloem transport of flowering signals. *Curr. Opin. Plant Biol.* **11**, 687–694.

Goncharov, N. (2004) Response to vernalization in wheat: its quantitative or qualitative nature. *Cereal Res. Commun.* **32**, 323–330.

Hanzawa, Y., Money, T. and Bradley, D. (2005) A single amino acid converts a repressor to an activator of flowering. *Proc. Natl. Acad. Sci. USA* **102**, 7748–7753.

Hill, J., Demarest, B., Bisgrove, B., Gorsi, B., Su, Y. and Yost, H. (2013) MMAPPR: mutation mapping analysis pipeline for pooled RNA-seq. *Genome Res.* **23**, 687–697.

Hou, C. and Yang, C. (2016) Comparative analysis of the pteridophyte Adiantum MFT ortholog reveals the specificity of combined FT/MFT C and N terminal interaction with FD for the regulation of the downstream gene AP1. *Plant Mol. Biol.* **91**, 563–579.

Ishida, Y., Tsunashima, M., Hiei, Y. and Komari, T. (2015) Wheat (*Triticum aestivum* L.) transformation using immature embryos. *Methods Mol. Biol.* **1223**, 189–193.

IWGSC (2018) Shifting the limits in wheat research and breeding using a fully annotated reference genome. *Science* **361**, aar7191.

Kamran, A., Iqbal, M. and Spaner, D. (2014) Flowering time in wheat (*Triticum aestivum* L.): a key factor for global adaptability. *Euphytica* **197**, 1–26.

Kim, D., Langmead, B. and Salzberg, S.L. (2015) HISAT: a fast spliced aligner with low memory requirements. *Nat. Methods* **12**, 357–360.

Kiseleva, A.A. and Salina, E.A. (2018) Genetic regulation of common wheat heading time. *Russ. J. Genet.* **54**, 375–388.

Köhler, C., Alvarez, M.A., Li, C., Lin, H., Joe, A., Padilla, M., Woods, D.P. *et al*. (2023) *EARLY FLOWERING 3* interactions with *PHYTOCHROME B* and *PHOTOPERIOD1* are critical for the photoperiodic regulation of wheat heading time. *PLoS Genet.* **19**, e1010655.

Langfelder, P. and Horvath, S. (2008) WGCNA: an R package for weighted correlation network analysis. *BMC Bioinformatics* **9**, 1–13.

Lee, A., Jung, H., Park, H.J., Jo, S.H., Jung, M., Kim, Y.S. and Cho, H.S. (2023) Their C-termini divide *Brassica rapa* FT-like proteins into FD-interacting and FD-independent proteins that have different effects on the floral transition. *Front. Plant Sci.* **13**, 1091563.

Li, C. and Dubcovsky, J. (2008) Wheat FT protein regulates *VRN1* transcription through interactions with FDL2. *Plant J.* **55**, 543–554.

Li, C., Lin, H. and Dubcovsky, J. (2015) Factorial combinations of protein interactions generate a multiplicity of florigen activation complexes in wheat and barley. *Plant J.* **84**, 70–82.

Li, G., Boontung, R., Powers, C., Belamkar, V., Huang, T., Miao, F., Baenziger, P.S. *et al*. (2017) Genetic basis of the very short life cycle of 'Apogee' wheat. *BMC Genomics* **18**, 838.

Li, Y., Xiong, H., Guo, H., Zhou, C., Fu, M., Xie, Y., Zhao, L. *et al*. (2023) Fine mapping and genetic analysis identified a C_2H_2-type zinc finger as a candidate gene for heading date regulation in wheat. *Theor. Appl. Genet.* **136**, 140.

Li, Y., Xiong, H., Guo, H., Zhou, C., Xie, Y., Zhao, L., Gu, J. *et al*. (2020) Identification of the vernalization gene *VRN-B1* responsible for heading date variation by QTL mapping using a RIL population in wheat. *BMC Plant Biol.* **20**, 331.

Liu, L., Liu, C., Hou, X., Xi, W., Shen, L., Tao, Z., Wang, Y. *et al*. (2012) FTIP1 is an essential regulator required for florigen transport. *PLoS Biol.* **10**, e1001313.

Liu, T., Liu, H., Zhang, H. and Xing, Y. (2013) Validation and characterization of *Ghd7.1*, a major quantitative trait locus with pleiotropic effects on spikelets

per panicle, plant height, and heading date in rice (*Oryza sativa* L.). *J. Integr. Plant Biol.* **55**, 917–927.

Livak, K.J. and Schmittgen, T.D. (2001) Analysis of relative gene expression data using real-time quantitative PCR and the $2^{-\Delta\Delta CT}$ Method. *Methods* **25**, 402–408.

Ma, J., Wang, Y., Ma, X., Meng, L., Jing, R., Wang, F., Wang, S. *et al*. (2019) Disruption of gene *SPL35*, encoding a novel CUE domain-containing protein, leads to cell death and enhanced disease response in rice. *Plant Biotechnol. J.* **17**, 1679–1693.

Mathieu, J., Warthmann, N., Kuttner, F. and Schmid, M. (2007) Export of FT protein from phloem companion cells is sufficient for floral induction in *Arabidopsis*. *Curr. Biol.* **17**, 1055–1060.

Meng, L., Li, H., Zhang, L. and Wang, J. (2015) QTL IciMapping: Integrated software for genetic linkage map construction and quantitative trait locus mapping in biparental populations. *Crop Journal* **3**, 269–283.

Mimida, N., Kidou, S.I., Iwanami, H., Moriya, S., Abe, K., Voogd, C., Varkonyi-Gasic, E. *et al*. (2011) Apple FLOWERING LOCUS T proteins interact with transcription factors implicated in cell growth and organ development. *Tree Physiol.* **31**, 555–566.

Mo, Y., Vanzetti, L.S., Hale, I., Spagnolo, E.J., Guidobaldi, F., Al-Oboudi, J., Odle, N. *et al*. (2018) Identification and characterization of *Rht25*, a locus on chromosome arm 6AS affecting wheat plant height, heading time, and spike development. *Theor. Appl. Genet.* **131**, 2021–2035.

Nakamura, Y., Lin, Y.C., Watanabe, S., Liu, Y.C., Katsuyama, K., Kanehara, K. and Inaba, K. (2019) High-resolution crystal structure of Arabidopsis FLOWERING LOCUS T illuminates its phospholipid-binding site in flowering. *iScience* **21**, 577–586.

Niwa, M., Daimon, Y., Kurotani, K., Higo, A., Pruneda-Paz, J.L., Breton, G., Mitsuda, N. *et al*. (2013) BRANCHED1 interacts with FLOWERING LOCUS T to repress the floral transition of the axillary meristems in Arabidopsis. *Plant Cell* **25**, 1228–1242.

Noh, Y.S., Bizzell, C.M., Noh, B., Schomburg, F.M. and Amasino, R.M. (2004) *EARLY FLOWERING 5* acts as a floral repressor in Arabidopsis. *Plant J.* **38**, 664–672.

Pertea, M., Pertea, G.M., Antonescu, C.M., Chang, T.-C., Mendell, J.T. and Salzberg, S.L. (2015) StringTie enables improved reconstruction of a transcriptome from RNA-seq reads. *Nat. Biotechnol.* **33**, 290–295.

Pfeifer, M., Kugler, K.G., Sandve, S.R., Zhan, B., Rudi, H., Hvidsten, T.R., Mayer, K.F. *et al*. (2014) Genome interplay in the grain transcriptome of hexaploid bread wheat. *Science* **345**, 1250091.

Ramirez-Gonzalez, R., Uauy, C. and Caccamo, M. (2015) PolyMarker: a fast polyploid primer design pipeline. *Bioinformatics* **31**, 2038–2039.

Shannon, P., Markiel, A., Ozier, O., Baliga, N.S., Wang, J.T., Ramage, D., Amin, N. *et al*. (2003) Cytoscape: a software environment for integrated models of biomolecular interaction networks. *Genome Res.* **13**, 2498–2504.

Shaw, L.M., Lyu, B., Turner, R., Li, C., Chen, F., Han, X., Fu, D. *et al*. (2019) *FLOWERING LOCUS T2* regulates spike development and fertility in temperate cereals. *J. Exp. Bot.* **70**, 193–204.

Shaw, L.M., Turner, A.S. and Laurie, D.A. (2012) The impact of photoperiod insensitive *Ppd-1a* mutations on the photoperiod pathway across the three genomes of hexaploid wheat (*Triticum aestivum*). *Plant J.* **71**, 71–84.

Sun, Y., Li, X., Zhang, Q., Zhang, X., Ma, Z., Hong, Y., Zhang, L. *et al*. (2023) The reverse mutation of CsMLO8 results in susceptibility to powdery mildew via inhibiting cell wall apposition formation and cell death in cucumber (*Cucumis sativus* L.). *Sci. Hortic.* **313**, 111894.

Taoka, K., Ohki, I., Tsuji, H., Furuita, K., Hayashi, K., Yanase, T., Yamaguchi, M. *et al*. (2011) 14-3-3 proteins act as intracellular receptors for rice Hd3a florigen. *Nature* **476**, 332–335.

Tian, H., Baxter, I.R., Lahner, B., Reinders, A., Salt, D.E. and Ward, J.M. (2010) *Arabidopsis* NPCC6/NaKR1 is a phloem mobile metal binding protein necessary for phloem function and root meristem maintenance. *Plant Cell* **22**, 3963–3979.

Trapnell, C., Williams, B.A., Pertea, G., Mortazavi, A., Kwan, G., van Baren, M.J., Salzberg, S.L. *et al*. (2010) Transcript assembly and quantification by RNA-Seq reveals unannotated transcripts and isoform switching during cell differentiation. *Nat. Biotechnol.* **28**, 511–515.

Wigge, P., Kim, M., Jaeger, K., Busch, W., Schmid, M., Lohmann, J. and Weigel, D. (2005) Integration of spatial and temporal information during floral induction in *Arabidopsis*. *Science* **309**, 1056–1059.

Wilhelm, E., Turner, A. and Laurie, D. (2009) Photoperiod insensitive *Ppd-A1a* mutations in tetraploid wheat (*Triticum durum* Desf.). *Theor. Appl. Genet.* **118**, 285–294.

Wu, J., Qiao, L., Liu, Y., Fu, B., Nagarajan, R., Rauf, Y., Jia, H. *et al*. (2022a) Rapid identification and deployment of major genes for flowering time and awn traits in common wheat. *Front. Plant Sci.* **13**, 992811.

Wu, J., Wu, Q., Bo, Z., Zhu, X., Zhang, J., Li, Q. and Kong, W. (2022b) Comprehensive effects of *Flowering Locus T*-mediated stem growth in tobacco. *Front. Plant Sci.* **13**, 922919.

Xiong, H., Guo, H., Fu, M., Xie, Y., Zhao, L., Gu, J., Zhao, S. *et al*. (2023) A large-scale whole-exome sequencing mutant resource for functional genomics in wheat. *Plant Biotechnol. J.* **21**, 2047–2056.

Xiong, H., Zhou, C., Fu, M., Guo, H., Xie, Y., Zhao, L., Gu, J. *et al*. (2022) Cloning and functional characterization of *Rht8*, a "Green Revolution" replacement gene in wheat. *Mol. Plant* **15**, 373–376.

Yan, L., Fu, D., Li, C., Blechl, A., Tranquilli, G., Bonafede, M., Sanchez, A. *et al*. (2006) The wheat and barley vernalization gene *VRN3* is an orthologue of *FT*. *Proc. Natl. Acad. Sci. USA* **103**, 19581–19586.

Yan, L., Loukoianov, A., Blechl, A., Tranquilli, G., Ramakrishna, W., SanMiguel, P., Bennetzen, J.L. *et al*. (2004) The wheat *VRN2* gene is a flowering repressor down-regulated by vernalization. *Science* **303**, 1640–1644.

Yan, L., Loukoianov, A., Tranquilli, G., Helguera, M., Fahima, T. and Dubcovsky, J. (2003) Positional cloning of the wheat vernalization gene *VRN1*. *Proc. Natl. Acad. Sci. USA* **100**, 6263–6268.

Yan, W., Zhang, Z.-H., Wang, K., Guo, L., Zhu, Y.-J., Fan, Y.-Y., Cheng, S.-H. *et al*. (2012) Pleiotropism of the photoperiod-insensitive allele of *Hd1* on heading date, plant height and yield traits in rice. *PLoS One* **7**, 1–6.

Yan, W.H., Wang, P., Chen, H.X., Zhou, H.J., Li, Q.P., Wang, C.R., Ding, Z.H. *et al*. (2011) A major QTL, *Ghd8*, plays pleiotropic roles in regulating grain productivity, plant height, and heading date in rice. *Mol. Plant* **4**, 319–330.

Zhang, X.K., Xiao, Y.G., Zhang, Y., Xia, X.C., Dubcovsky, J. and He, Z.H. (2008) Allelic variation at the vernalization genes *Vrn-A1*, *Vrn-B1*, *Vrn-D1*, and *Vrn-B3* in Chinese wheat cultivars and their association with growth habit. *Crop Sci.* **48**, 458–470.

Zhu, Y., Liu, L., Shen, L. and Yu, H. (2016) NaKR1 regulates long-distance movement of FLOWERING LOCUS T in *Arabidopsis*. *Nature Plants* **2**, 16075.

Zhu, Y.-J., Fan, Y.-Y., Wang, K., Huang, D.-R., Liu, W.-Z., Ying, J.-Z. and Zhuang, J.-Y. (2017) Rice *Flowering Locus T 1* plays an important role in heading date influencing yield traits in rice. *Sci. Rep.* **7**, 1–10.

Zikhali, M., Wingen, L.U. and Griffiths, S. (2016) Delimitation of the *Earliness per se D1* (*Eps-D1*) flowering gene to a subtelomeric chromosomal deletion in bread wheat (*Triticum aestivum*). *J. Exp. Bot.* **67**, 287–299.

Supporting information

Additional supporting information may be found online in the Supporting Information section at the end of the article.

Figure S1 Phenotypic comparison of the early heading mutant *eh1* and WT.

Figure S2 Evaluation of *FT-D1*^{eh1} on HD, plant height, and spike architecture in backcrossed and homozygous $F_{2:3}$ lines.

Figure S3 Both FT-D1 alleles from *eh1* and WT were capable of interacting with TaNaKR5 and TaFTIP7.

Figure S4 Sequence alignment of wheat FT-D1, rice Hd3a, and *Arabidopsis* FT.

Figure S5 Yeast two-hybrid assays validated protein–protein interactions between different truncated FT-D1 proteins and FDL6, TaNaKR5, and TaFTIP7, respectively.

Figure S6 DNA sequence alignment of *FT-D1*^{eh1}, *FT-D1*^{WT} and *FT-D1*^{Fielder}.

Figure S7 The triple mutant *ft1-aabbDd*^{KO} failed to flower and produce seeds in the whole developmental stage.

Figure S8 Phenotype of the *FT-D1*^{eh1} overexpression lines at the callus differentiation stage.

Figure S9 Validation of positive *FT-D1* transgenic lines.

Figure S10 Phenotype of the florets in *ft-D1*^{KO} and *FT-D1*^{OE} lines at the same developmental stage.
Figure S11 Tissue-specific expressions of *ELF5-2A* (*TraesCS2A01G245500*) at different vegetative growth stages.
Figure S12 TILLING mutants with functional mutations in *ELF5-2A* and *ELF5-2B* displayed delayed HD as compared with the wild-type Jing411.
Figure S13 Both TaNaKR5 and TaFTIP7 are important to FT-D1 accumulation in wheat spikes.
Table S1 SNPs and Indels identified in the candidate mapping region of *eh1*.
Table S2 Summary of RNA-seq data generated from *FT-D1* KO and OE lines.
Table S3 DEGs identified from the *ft-D1*^{KO} and *FT-D1*^{OE} transgenic lines.
Table S4 The gene list of WGCNA modules.
Table S5 List of hub genes identified from WGCNA.
Table S6 SNPs and Indels identified in the *eh1* mutant by exome capturing sequencing.
Table S7 Primer sequences used in this study.